KSME

Springer

Journal of Mechanical Science and Technology 34 (2) 2020

Original Article
DOI 10.1007/s12206-020-0109-4

Keywords:
· Hydrostatic guideway
· Motion accuracy
· Motion error
· Relative difference
· Guide rail
· Numerical computation
· Pose

Correspondence to:
Zhenzhong Wang
wangzhenzhong@xmu.edu.cn

Citation:
Shi, C., Wang, Z., Peng, Y. (2020). Influence of relative difference between paired guide rails on motion accuracy in closed hydrostatic guideways. Journal of Mechanical Science and Technology 34 (2) (2020) 631~648.
http://doi.org/10.1007/s12206-020-0109-4

Received August 28th, 2019
Revised December 9th, 2019
Accepted December 19th, 2019

† Recommended by Editor
No-cheol Park

Influence of relative difference between paired guide rails on motion accuracy in closed hydrostatic guideways

Chenchun Shi, Zhenzhong Wang and Yunfeng Peng

Department of Mechanical and Electrical Engineering, Xiamen University, Xiamen 361005, China

Abstract There have been many researches concerning the motion errors of hydrostatic guideways because they directly affect the accuracy of machined parts. Actually, each paired guide rail has its own profile feature, and the position error also cannot be zero, so the relative difference between guide rails should not be neglected. In this paper, a typical closed hydrostatic guideway with four pads is taken as the sample, and the quasi-static analysis model is directly developed by incorporating the concept of pose, which is then employed to study the effect of relative difference on motion accuracy in the field of hydrostatic guideways. The numerical results demonstrate that, the greater the amplitude deviation, the larger the motion errors, while the influence of the wavelength deviation on motion accuracy exhibits regularity only within some intervals, the phase deviation mainly affects the angular but not the linear motion error, the influence from the parallelism error is not significant. Moreover, it is figured out that the fluctuation of the difference between the average film thicknesses of two adjacent pads does result in the variation of the motion errors, the greater the fluctuation, the larger the motion errors. The revealed mechanisms are expected to be valuable for designers.

1. Introduction

Hydrostatic guideways are widely applied as the vital functional unit in precision and ultra-precision machine tools for their low running friction, high stiffness, high motion accuracy, superior vibration-resistance, excellent adaptability, virtually no wear, long service life, etc [1-6]. Since the motion errors of hydrostatic guideways directly affect the accuracy of the machined parts [5, 7], the research efforts of many scholars have been focused on the motion accuracy of hydrostatic guideways. Refs. [2, 8, 9] have suggested that the motion errors of hydrostatic guideways are relevant to the profile errors of guide rails tightly. Zha et al. [10] established a static analysis model of open hydrostatic guideways with four pads, and the effect of the ratio of pad center spacing to guide rail profile error wavelength on motion accuracy was the primary focus, but the influence of relative difference between guide rails on motion accuracy seemed not to be involved. Although the research conducted by Zha et al. [5] presented an approach to model and compensate the vertical straightness error of gantry type open hydrostatic guideways with four pads, the profile errors of two guide rails were assumed to be the same with each other in the simulation, that is, the three main parameters (wavelength, amplitude and phase) of one guide rail's profile error were considered to be consistent with those of the other rail's, respectively. Xue et al. [6, 11] investigated the error averaging effect of the typical closed hydrostatic guideway with four pads theoretically by averaging the oil film thickness on a pad, and proposed some suggestions to improve the motion accuracy, nevertheless, the difference of profile errors between the paired guide rails were also not taken into account. Wang et al. [8] studied the effect of speed on motion errors in the closed hydrostatic guideway with four pads, but it was still based on the assumption that the three main parameters of one guide rail's profile error were equal to those of the other paired rail's, respectively. Shamoto et al. [12] analyzed the relationship between the film reaction force in a single pad and the profile error of a

guide rail at various spatial frequencies by FEM, and developed the analysis model for motion errors based on the transfer function method (TFM), even so, the difference of profile errors between guide rails were not reported thoroughly. In practice, each guide rail does have its own profile feature, and the profile errors of these rails are not the same with each other exactly [5]. Additionally, there is very little information available in literature about the influence of the relative geometry position error between guide rails on motion accuracy. It is the manufacture and assembly of hydrostatic guideways that cause the profile error and position error, respectively. Both of the two errors are determined as the relative difference between guide rails in this study.

Among the aforementioned researches, TFM and the simplification of oil film as the linear spring element are known as the main analysis methods. However, the former corresponds to that the hydrostatic guideways are considered as the linear system, actually, they are supposed to be nonlinear. Also, this method itself is complex and not convenient to be used in practical application [9]. The latter takes the oil film stiffness of pads into account only, according to Refs. [13, 14], the damping term could not be neglected. Despite the motion errors can be analyzed by applying FEA to the entire hydrostatic table under equilibrium conditions, the model may become quite cumbersome and complex, and is difficult to apply to various types of tables [15]. The pose description is commonly known such as in robot kinematics, but rarely adopted for the research of motion accuracy in hydrostatic guideways. Accordingly, by introducing the concept of pose, one analysis model with less simplification directly calculating and studying the motion errors of hydrostatic guideways is deserved to be developed as soon as possible.

Hydrostatic guideways do play an important role in determining the accuracy of precision and ultra-precision machine tools. The design of hydrostatic guideways extensively depends on the knowledge and experience of the designer [16]. However, the designer does not have the theoretical analysis tools to calculate the accuracy quantitatively, so the accuracy is usually estimated empirically or experimentally in the design process, therefore, a theoretical and quantitative assessment of the accuracy before fabrication could be very effective [15, 17, 18]. Kim et al. [19] also have pointed out that, in order to reduce time and cost, the theoretical analysis tools to predict the accuracy of these machine tools in the design process are necessary. Besides, if the motion errors can be predicted from the rail profile in the design step, the allowable tolerance of the rail profile error could be assessed before fabrication, and the time for finishing process could be reduced greatly [15]. For example, aiming to optimize the structural and accuracy design of hydrostatic guideways, the theoretical researches on the error averaging effect of hydrostatic guideways were carried out by Xue et al. [6, 11], but these theoretical analyses failed to take the relative difference between paired guide rails into account, and the oil film also was directly simplified as the linear spring element. Hence, the related theoretical researches are essential and still desired to be done further.

Large optical ultra-precision grinding machine is usually seen as the core equipment for astronomical mirror machining due to that it determines the efficiency of the whole process [16]. An ultra-precision grinding machine UPG 80 for large scale optical aspheric lens is being developed by our assignment group, the maximum size of the machined workpiece can be 1300 mm×750 mm×550 mm, and the surface figure of 530 mm×530 mm aspheric workpiece is required as PV (peak-to-valley) ≤ 5 μm. Among all the parts of a large optical ultra-precision grinding machine, the performances of the guideways do play a significant role, because it influences the axial accuracy directly [16, 20]. In UPG 80, the closed hydrostatic guideways are adopted, and the accuracy of the machined workpieces are directly affected by the motion errors of these hydrostatic guideways, accordingly, a typical closed hydrostatic guideway with four pads is taken as the sample in our study. By introducing the concept of pose commonly known in robot kinematics, the pose of moving hydrostatic table can be described, and the quasi-static analysis model is developed directly, which is then employed to study the effect of relative difference between paired guide rails on motion accuracy of hydrostatic guideways. The findings and mechanisms presented in this paper are expected to provide theoretical references for precision design of hydrostatic guideways including UPG 80.

2. Modeling

The configuration of UPG 80 can be seen from Fig. 1, and each of the three linear axes in UPG 80 uses the closed hydrostatic guideways. Take the *X* axis as the instance, the table and those hydrostatic guide shoes (HGSs) shown in Fig. 1(c) are connected by bolts, which forms the hydrostatic table, and it can be driven by ballscrew. The structure of *X* axis depicted simplistically in Fig. 2 is a typical closed hydrostatic guideway with four pads. Note that, this structure also is commonly adopted in other researches [6, 8, 9, 11]. In this paper, the typical closed hydrostatic guideway with four pads shown in Fig. 2 will be taken as the sample, and the corresponding quasi-static analysis model is established to study the influence of relative difference between paired rails on motion accuracy further.

2.1 Closed hydrostatic guideway with four pads

Fig. 2(a) shows the structure of hydrostatic table, and its length, width and height are denoted by *L*, *H* and *B*, respectively. The four rectangular pads are distributed symmetrically, and both the size and structure of these pads are the same with each other. The center spacing between two adjacent pads is denoted by *l*. Fig. 2(b) shows one of the four rectangular pads alone the negative direction of Z_A axis, the length and width of pad are *M* and *W*, while those of recess are *M*-2*m* and

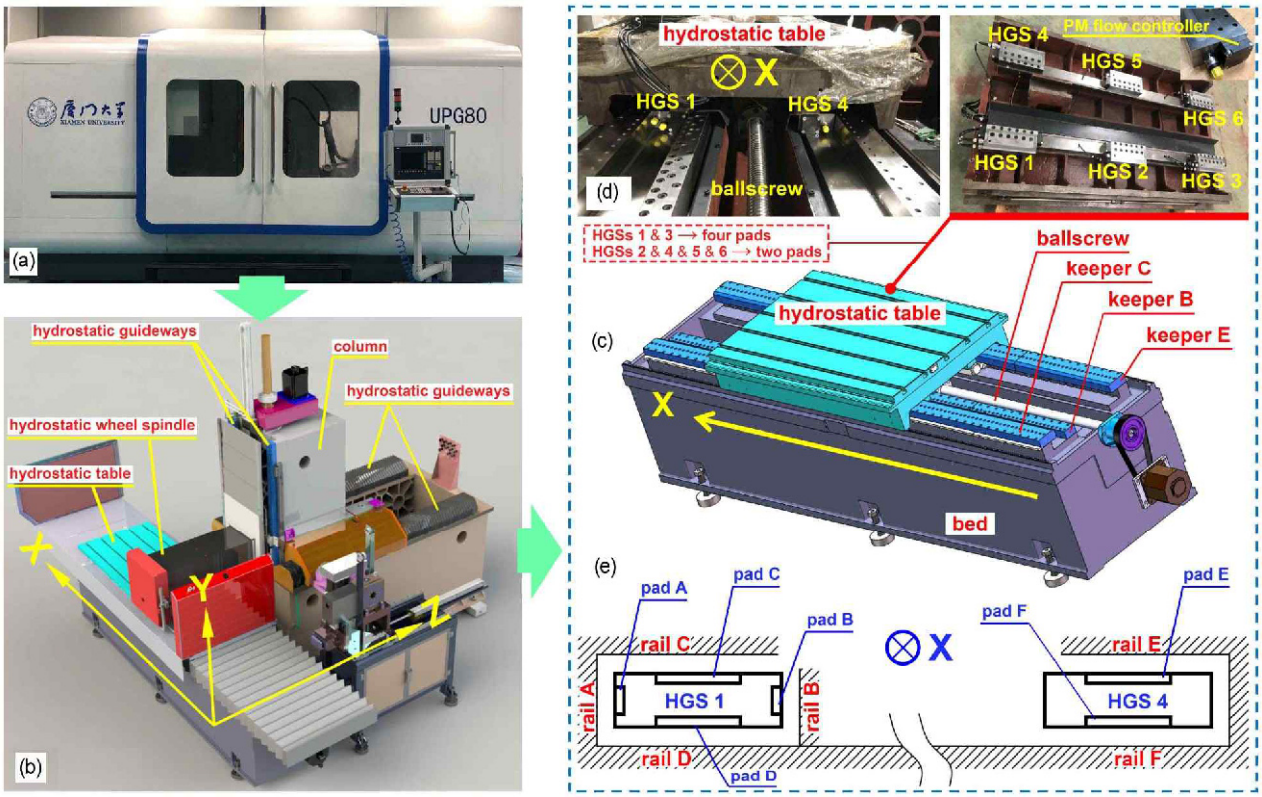

Fig. 1. Configuration of UPG 80: (a) With the shield; (b) without the shield; (c) bed and hydrostatic table of X axis; (d) without keepers C and E; (e) closed hydrostatic guideways of X axis.

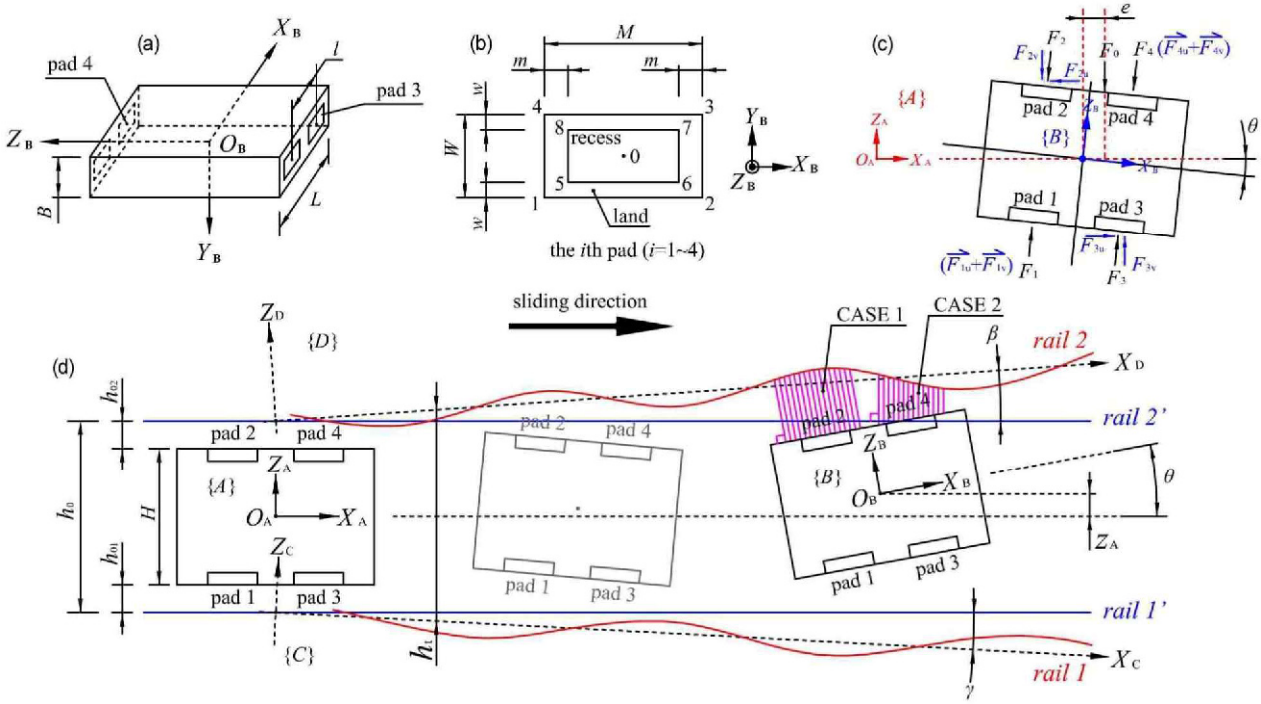

Fig. 2. Typical closed hydrostatic guideway with four pads: (a) Structure of hydrostatic table; (b) rectangular pad; (c) force analysis of general equilibrium state; (d) pose of hydrostatic table.

W-2*w*, respectively. Point 0 to point 8 are the nine points all located in the pad plane.

As shown in Fig. 2(d), due to the manufacturing error, the profiles of the paired rails in actual engineering cannot be flat but curved. Same to Refs. [6, 8, 10, 11], it is also considered here that the profile error of guide rail does not change along the width direction (the direction of Y_A axis), and the profile error function of rail 1 can be mathematically described as

$$Z_1 = E_1 \sin\left(\frac{2\pi}{\lambda_1}\cdot X + \varphi_1\right) \tag{1}$$

where E_1, λ_1, φ_1 denote the amplitude, wavelength, and phase, respectively. Similarly, that of rail 2 is given as

$$Z_2 = E_2 \sin\left(\frac{2\pi}{\lambda_2}\cdot X + \varphi_2\right) \tag{2}$$

It is rail 1 and rail 2 that are paired. Eqs. (1) and (2) has not taken the relative geometry position error between the paired rails into account yet, however, the position error induced by the assembly error does exist in actual engineering. Therefore, the parallelism error between rail 1 and rail 2 representing the position error must to be considered in order to obtain the general functions of the actual paired guide rails with profile errors.

As shown in Fig. 2(d), the profiles of both rail 1' and rail 2' are flat, and the relative geometry position error between them also is zero, so they two are named as ideal rails. However, there exists a nonzero angle between the neutral plane of the actual rail's profile and that of the ideal rail's. It is this nonzero angle that results in the parallelism error. Here, the space rectangular coordinate systems {*A*}, {*B*}, {*C*} and {*D*} are introduced as the reference coordinate system, the hydrostatic table coordinate system, the neutral plane coordinate systems of rail 1 and rail 2, respectively. Points O_A, O_C and O_D are all located on Z_A axis. The distance of rail 1' from the plane $O_AX_AY_A$ is $h_0/2$, and so is rail 2'. Take rail 2 as the example, the neutral plane of its profile just is the plane $O_DX_DY_D$, the descriptions of point $\boldsymbol{p}$ on the curved profile in {*A*} and {*D*} are different and denoted by ${}^{A}\boldsymbol{p}$ and ${}^{D}\boldsymbol{p}$, respectively. Based on the concept of pose commonly known such as in robot kinematics [21], then the relationship between ${}^{A}\boldsymbol{p}$ and ${}^{D}\boldsymbol{p}$ can be expressed as

$${}^{A}\boldsymbol{p} = {}^{A}_{D}\boldsymbol{R}\,{}^{D}\boldsymbol{p} + {}^{A}\boldsymbol{p}_{Do} \tag{3}$$

where ${}^{A}_{D}\boldsymbol{R}$ is the rotation matrix and represents the orientation of {*D*} relative to {*A*}, ${}^{A}\boldsymbol{p}_{Do}$ is the translation vector of {*D*} relative to {*A*}. The expressions of ${}^{A}_{D}\boldsymbol{R}$, ${}^{A}\boldsymbol{p}_{Do}$ and ${}^{D}\boldsymbol{p}$ are

$${}^{A}_{D}\boldsymbol{R} = \begin{bmatrix} \cos\beta & 0 & \sin\beta \\ 0 & 1 & 0 \\ -\sin\beta & 0 & \cos\beta \end{bmatrix} \tag{4}$$

$${}^{A}\boldsymbol{p}_{Do} = \begin{bmatrix} 0 \\ 0 \\ h_0/2 \end{bmatrix} \tag{5}$$

$${}^{D}\boldsymbol{p} = \begin{bmatrix} {}^{D}X \\ 0 \\ {}^{D}Z_2 \end{bmatrix} = \begin{bmatrix} {}^{D}X & 0 & E_2\sin\left(\dfrac{2\pi\cdot {}^{D}X}{\lambda_2} + \varphi_2\right) \end{bmatrix}^{\mathrm{T}} \tag{6}$$

Substituting Eqs. (4)-(6) into Eq. (3), then ${}^{A}\boldsymbol{p}$ can be solved as

$$\begin{aligned} {}^{A}\boldsymbol{p} &= \begin{bmatrix} {}^{A}X \\ {}^{A}Y \\ {}^{A}Z_2 \end{bmatrix} \\ &= \begin{bmatrix} \cos\beta\cdot {}^{D}X + \sin\beta\cdot E_2\sin\left(\dfrac{2\pi\cdot {}^{D}X}{\lambda_2} + \varphi_2\right) \\ 0 \\ -\sin\beta\cdot {}^{D}X + \cos\beta\cdot E_2\sin\left(\dfrac{2\pi\cdot {}^{D}X}{\lambda_2} + \varphi_2\right) + \dfrac{h_0}{2} \end{bmatrix} \end{aligned} \tag{7}$$

Eq. (7) is the general mathematical description of rail 2 in {*A*}. Here, ${}^{D}X$ can be seen as the intermediate variable. By eliminating ${}^{D}X$, Eq. (7) also can be expressed as

$$\begin{aligned} &{}^{A}X\sin\beta + {}^{A}Z_2\cos\beta \\ &= E_2\sin\left[\frac{2\pi}{\lambda_2}\cdot\left({}^{A}X\cos\beta - {}^{A}Z_2\sin\beta + \frac{h_0\sin\beta}{2}\right) + \varphi_2\right] \\ &+ \frac{h_0\cos\beta}{2} \end{aligned} \tag{8}$$

Similarly, that of rail 1 in {*A*} is written as

$$\begin{aligned} &{}^{A}X\sin\gamma + {}^{A}Z_1\cos\gamma \\ &= E_1\sin\left[\frac{2\pi}{\lambda_1}\cdot\left({}^{A}X\cos\gamma - {}^{A}Z_1\sin\gamma + \frac{h_0\sin\gamma}{2}\right) + \varphi_1\right] \\ &- \frac{h_0\cos\gamma}{2} \end{aligned} \tag{9}$$

Eqs. (8) and (9) are implicit functions. Especially, if both the angles β and γ shown in Fig. 2(d) are set as zero, then the parallelism error is eliminated, and the explicit expressions of rail 1 and rail 2 are obtained as

$${}^{A}Z_1 = E_1\sin\left[\frac{2\pi}{\lambda_1}\cdot {}^{A}X + \varphi_1\right] - \frac{h_0}{2} \tag{10}$$

$${}^{A}Z_2 = E_2\sin\left[\frac{2\pi}{\lambda_2}\cdot {}^{A}X + \varphi_2\right] + \frac{h_0}{2} \tag{11}$$

It should be pointed out that the space rectangular coordi-

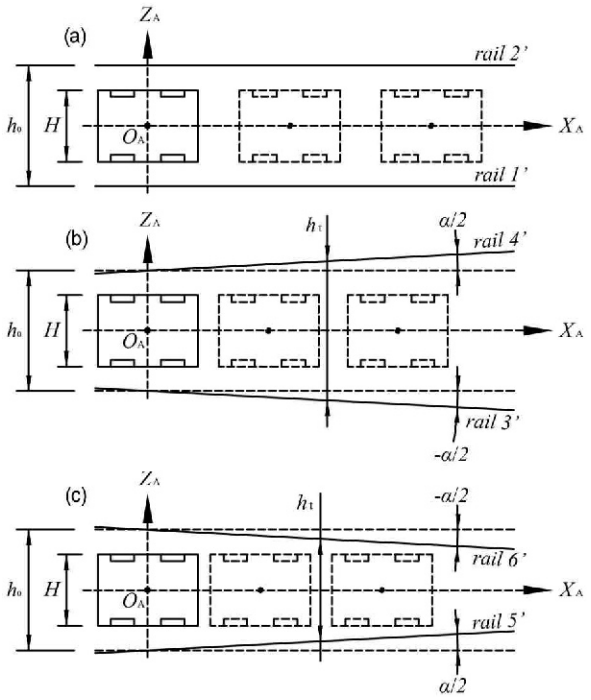

Fig. 3. Three cases of the relative position between the ideal paired rails: (a) Rectilinear shape; (b) positive flared shape; (c) negative flared shape.

nate system of UPG 80 shown in Fig. 1 is different with those depicted in Fig. 2.

2.2 Quasi-static motion analysis

Same to Refs. [6, 9], the hydrostatic table in this paper also is under quasi-static condition which means the moving speed is quite slow. As shown in Figs. 2(c) and (d), when the external force F_0 acting on the hydrostatic table is constant and the paired rails both are ideal, the four oil film reaction forces F_1 to F_4 are all invariant, and the resultant force and resultant moment applied to the table equal to zero, so the motion errors are non-existent. Furthermore, if F_0 is set as zero and those restrictors corresponding to the four pads are also the same with each other, then the clearance between any pad and its matched ideal rail is always $(h_0\text{-}H)/2$, in other words, no matter where the table moves to along the direction of X_A axis, $h_{01} = h_{02} = (h_0\text{-}H)/2$, and the table is defined to be in special equilibrium state. In engineering, the profile errors and relative position error of one paired guide rails in closed hydrostatic guideways cannot be zero, so the hydrostatic table moves and swings simultaneously, which correspond to the linear motion error z_A and the angular motion error θ, respectively. In this situation, the table is defined to be in general equilibrium state. No matter which equilibrium state it is, both of the resultant force and resultant moment on the hydrostatic table are zero.

Fig. 3 depicts three cases of the relative position between the ideal paired rails, they are named as rectilinear shape shown in Fig. 3(a), positive flared shape shown in Fig. 3(b) and negative flared shape shown in Fig. 3(c), respectively. As shown in Fig. 3(a), the paired guide rails without profile errors are parallel to each other, and the hydrostatic table is considered to be in special equilibrium state. When this same table performs in the positive flare shaped closed hydrostatic guideway shown in Fig. 3(b), the oil film thicknesses of two opposed oil pads always equal to each other, and the value can be calculated as $[h_t\ ({}^A p_{i0x})\text{-}H]/2$, where $h_t\ ({}^A p_{i0x})$ changes with the moving of the hydrostatic table, and ${}^A p_{i0x}$ denotes x coordinate of point 0 in the ith pad plane. Here, the hydrostatic table is defined to be in intermediate equilibrium state, so is the hydrostatic table shown in Fig. 3(c). The X_A axis is taken as the reference, so the motion errors of hydrostatic table in intermediate and special equilibrium state both are zero. Note that, the angles β in Eq. (8) and γ in Eq. (9) are supposed to change equally but reversely, then the X_A axis is determined as the reference. In our research, aiming to study the influence of the parallelism error between paired rails on motion accuracy in closed hydrostatic guideway, the values of β and γ are set as $\alpha/2$ and $-\alpha/2$, respectively. Thus, when $\alpha<0$, it is positive flared shape, and h_t increases linearly from $h_t\ ({}^A X = 0) = h_0$ along the positive direction of X_A axis. But when $\alpha>0$, it is negative flared shape, and h_t decreases linearly from $h_t\ ({}^A X = 0) = h_0$ along the positive direction of X_A axis. When $\alpha = 0$, h_t always equals to h_0 at any ${}^A X$ coordinate.

The space rectangular coordinate systems $\{B\}$ is established for the hydrostatic table in general equilibrium state, as shown in Fig. 2(d), and the origin O_B is fixed at the center of the table. Still take $\{A\}$ as the reference, based on the concept of pose [21] again, then the pose of hydrostatic table can be described directly. The descriptions of point $\boldsymbol{q}$ on the hydrostatic table in $\{A\}$ and $\{B\}$ are different and denoted by ${}^A\boldsymbol{q}$ and ${}^B\boldsymbol{q}$, respectively. The relationship between them can be given as

$$ {}^A\boldsymbol{q} = {}^A_B R\, {}^B\boldsymbol{q} + {}^A\boldsymbol{q}_{Bo} \tag{12} $$

where ${}^A_B\boldsymbol{R}$ is the rotation matrix and represents the orientation of $\{B\}$ relative to $\{A\}$, ${}^A\boldsymbol{q}_{Bo}$ is the translation vector of $\{B\}$ relative to $\{A\}$. So the mathematical expressions of ${}^A_B\boldsymbol{R}$ and ${}^A\boldsymbol{q}_{Bo}$ are

$$ {}^A_B\boldsymbol{R} = \begin{bmatrix} \cos\theta & 0 & \sin\theta \\ 0 & 1 & 0 \\ -\sin\theta & 0 & \cos\theta \end{bmatrix} \tag{13} $$

$$ {}^A\boldsymbol{q}_{Bo} = \begin{bmatrix} x_A \\ 0 \\ z_A \end{bmatrix} \tag{14} $$

Here, i denotes the number of pad, whereas j denotes the number of point in one pad plane. So there have $i = 1\sim4$ and $j = 0\sim8$. ${}^A\boldsymbol{q}_{ij}$ and ${}^B\boldsymbol{q}_{ij}$ are the coordinates of the jth point in the ith pad plane in $\{A\}$ and $\{B\}$, respectively. For instance, ${}^B\boldsymbol{q}_{10}$ can be expressed as

$$ {}^{B}\boldsymbol{q}_{10}=\left[-\frac{l}{2}\quad 0\quad -\frac{H}{2}\right]^{\mathrm{T}} \tag{15} $$

Then, according to Eqs. (12)-(14), there has

$$ \begin{aligned} {}^{A}\boldsymbol{q}_{10}&=\begin{bmatrix} {}^{A}q_{10x}\\ {}^{A}q_{10y}\\ {}^{A}q_{10z}\end{bmatrix}={}^{A}_{B}\boldsymbol{R}\,{}^{B}\boldsymbol{q}_{10}+{}^{A}\boldsymbol{q}_{Bo}\\ &=\begin{bmatrix}\cos\theta & 0 & \sin\theta\\ 0 & 1 & 0\\ -\sin\theta & 0 & \cos\theta\end{bmatrix}\cdot\begin{bmatrix}-l/2\\ 0\\ -H/2\end{bmatrix}+\begin{bmatrix}x_{\mathrm{A}}\\ 0\\ z_{\mathrm{A}}\end{bmatrix}\\ &=\begin{bmatrix}x_{\mathrm{A}}-\dfrac{l}{2}\cos\theta-\dfrac{H}{2}\sin\theta\\ 0\\ z_{\mathrm{A}}-\dfrac{H}{2}\cos\theta+\dfrac{l}{2}\sin\theta\end{bmatrix}\end{aligned} \tag{16} $$

The corresponding relationship between ${}^{B}\boldsymbol{q}_{ij}$ and ${}^{A}\boldsymbol{q}_{ij}$ has been given in Appendix A.1. In addition, pad 1 and pad 3 are in the same plane, and the corresponding mathematical equation can be denoted by ${}^{A}Z_{13}$, similarly, ${}^{A}Z_{24}$ is obtained. Therefore, they two can be written as

$$ {}^{A}Z_{13}=-\tan\theta\cdot{}^{A}X+\tan\theta\cdot{}^{A}p_{10x}+{}^{A}p_{10z} \tag{17} $$

$$ {}^{A}Z_{24}=-\tan\theta\cdot{}^{A}X+\tan\theta\cdot{}^{A}p_{20x}+{}^{A}p_{20z} \tag{18} $$

What should be pointed out further is that, if Eqs. (17) and (18) are considered as the two-dimensional linear equations in plane $O_{\mathrm{A}}X_{\mathrm{A}}Z_{\mathrm{A}}$ equivalently, then the slopes of those two straight lines both are -tan θ, and its value is negative when $\theta > 0$, but positive when $\theta < 0$.

2.3 Static equilibrium

Both the resultant force and resultant moment of the hydrostatic table must equal to zero wherever it moves [5, 6, 10], which is called as static equilibrium in this paper. As shown in Figs. 2(c) and (d), the force equilibrium equation and the moment equilibrium equation are expressed as

$$ \begin{aligned} &F_{4\mathrm{v}}+F_{2\mathrm{v}}+F_0=F_{1\mathrm{v}}+F_{3\mathrm{v}}\Rightarrow\\ &F_4\cos\theta+F_2\cos\theta+F_0=F_1\cos\theta+F_3\cos\theta \end{aligned} \tag{19} $$

$$ \begin{aligned} &M_{O_{\mathrm{B}}Y_{\mathrm{B}}}=0\Rightarrow\\ &F_0\cdot e+F_4\cdot\frac{l}{2}+F_1\cdot\frac{l}{2}=F_2\cdot\frac{l}{2}+F_3\cdot\frac{l}{2} \end{aligned} \tag{20} $$

where F_i (i = 1~4) is the oil film reaction force on the ith pad, F_0 is the external force always parallel to Z_{A} axis, e is the arm of F_0. By solving the nonlinear equations consisting of Eqs. (19) and (20), the two motion errors at ${}^{A}X = x_{\mathrm{A}}$ can be obtained, and the corresponding variation trends also can be drawn. The solution of F_i is essential. Based on Refs. [4, 10, 22, 23], the oil film reaction force on the pad can be obtained as the product of the hydrostatic pressure in the recess P_{r} and the effective bearing area of the rectangle pad A_{e}.

Solving P_{r} is the first step. As shown in Fig. 1(c), the progressive mengen (PM) flow controllers are adopted in closed hydrostatic guideways of UPG 80. PM controller is the product of Hyprostatik Company in Germany and belongs to the membrane-type restrictor, which has been widely used as the key component in other precision machine tools [23-25]. Its structure and working principle can be easily found in Refs. [22, 23]. Here, just give the flow equation of the PM controller as following

$$ Q=Q_0\left(1+\frac{K_{\mathrm{r}}-1}{P_{\mathrm{s}}}\cdot P_{\mathrm{r}}\right) \tag{21} $$

where Q is the flow rate corresponding to P_{r}, Q_0 is the flow rate for P_{r} = 0, K_{r} is a characteristic parameter of PM controller and named as flow ratio, P_{s} is the supply pressure. There are three constraints should be concerned, the first is K_{r}>1.2, the second is 0.9P_{s}-P_{r}>0, and the last is P_{r}>0. The former two guarantee the normal performance of PM controller [22, 23]. The third constraint refers to that the orientation of every oil film reaction force does point to the pad plane perpendicularly, as shown in Fig. 2(c). Besides, one restrictor corresponds to one pad, and the four PM controllers of the hydrostatic table shown in Fig. 2(d) are all set as the same in our study, so there are

$$ Q_{0i}=Q_0,\quad K_{\mathrm{r}i}=K_{\mathrm{r}},\quad P_{\mathrm{s}i}=P_{\mathrm{s}},\quad i=1\sim 4 \tag{22} $$

From Refs. [22, 26], when the oil film thickness on one pad is h, then Q can be calculated as

$$ Q=\frac{P_{\mathrm{r}}}{R(h)} \tag{23} $$

where $R(h)$ is related to h and denotes the flow resistance of the land. However, h does refer to the clearance between the pad plane and its matched ideal rail without errors, which also is called as nominal oil film thickness [10]. Actually, as analyzed above, the moving hydrostatic table is in general equilibrium state, the angular motion error θ does exist, and the profile of guide rail also is not ideal but curved. Thus, h usually is replaced by the average oil film thickness h_a [5, 10, 11], and there is

$$ R(h)=\underset{(i=1\sim 4)}{R(h_{ai})}=\frac{3\eta}{{h_{ai}}^{3}\cdot\left(\dfrac{M-m}{4w}+\dfrac{W-w}{4m}\right)} \tag{24} $$

Combining Eqs. (21)-(24), the hydrostatic pressure in the recess is obtained as

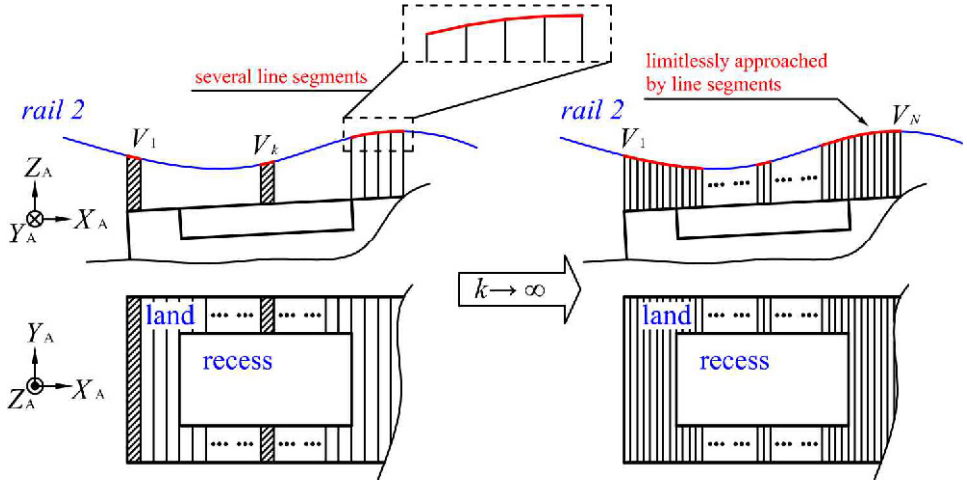

Fig. 4. Schematic diagram of calculating the average oil film thickness.

$$\begin{aligned}\left(\underset{i=1\sim4}{P_{ri}}\right) &= \frac{Q_{0i}\cdot R(h_{ai})}{1-\dfrac{Q_{0i}\cdot(K_{ri}-1)}{P_{si}}\cdot R(h_{ai})} \\ &= \frac{Q_0\cdot R(h_{ai})}{1-\dfrac{Q_0\cdot(K_r-1)}{P_s}\cdot R(h_{ai})}\end{aligned} \tag{25}$$

The second step is to calculate A_e, and it can be given by [4, 10, 23, 25]

$$A_{ei}(i=1\sim4)=(W-w)\cdot(M-m) \tag{26}$$

Combining Eqs. (25) and (26), there has

$$F_i(i=1\sim4)=P_{ri}\cdot A_{ei} \tag{27}$$

Finally, substituting Eq. (27) into the nonlinear equations consisting of Eqs. (19) and (20), the motion errors z_A and θ at any x_A coordinate can be determined. Both of the two motion errors can be effective under the three constraints mentioned above, otherwise, those design parameters involved in hydrostatic guideways need to be adjusted. Next, the calculation of average oil film thickness ha will be given.

2.4 Average oil film thickness

Average oil film thickness calculation method considering guide rail profile error has been proposed in Refs. [5, 6, 10, 11], and it can be understood as the average clearance between the land of pad and the matched guide rail. Similar method is adopted in this paper to obtain the four average oil film thicknesses of hydrostatic table in general equilibrium state. As shown in Fig. 2(d), CASE 1 denotes that the orientation of h_a is perpendicular to the pad plane, but to X_A axis in CASE 2. It is CASE 1 that should have been chosen to calculate h_a, whereas it requires {*B*} as the reference, which leads to that the profile error function of guide rail becomes a transcendental equation, so the analytical solutions cannot be got, furthermore, the unknown variables of z_A and θ involved in that transcendental equation also results in the non-existence of numerical solutions. If CASE 2 is chosen, then {*A*} becomes the reference, and as long as θ is small enough, the calculation accuracy can be guaranteed. Indeed, θ is very small and its order of magnitude generally is angular second. For example, sin θ usually is replaced by θ to improve those analysis models [8, 10]. Thus, CASE 2 is chosen to determine average oil film thickness in this paper.

As is seen from Eqs. (8) and (9), neither of them can be explicitly expressed, but both ${}^AZ_1$ and ${}^AZ_2$ at any x_A coordinate still can be obtained by numerical computation. Fig. 4 shows the schematic diagram of calculating the average oil film thickness, based on the limit theory, there is

$$\begin{aligned}h_a &= \lim_{N\to\infty}\sum_{k=1}^{N}\frac{V_k}{A_{\text{land}}} \\ &= \lim_{N\to\infty}\sum_{k=1}^{N}\frac{V_k}{2w\left({}^Aq_{12x}-{}^Aq_{11x}\right)+2(W-2w)\left({}^Aq_{12x}-{}^Aq_{16x}\right)}\end{aligned} \tag{28}$$

where A_{land} denotes the projected area of land in the plane $O_AX_AY_A$, and $A_{\text{land}} = A_{\text{land}i}$ (i = 1~4). When the profile of guide rail is divided into N segments, and N tends to infinity, the curved profile can be limitless approached by those line segments, as shown in Fig. 4. Accordingly, h_a can be obtained.

The relationship between the four oil film reaction forces and the two motion errors can be illustrated in detail as follow: Oil film reaction force F_i → Hydrostatic pressure in the recess P_{ri} → Flow resistance of the land R (h_{ai}) → Average oil film thickness h_{ai} → Motion position of the hydrostatic table and the motion errors (x_A, z_A, θ).

Table 1. Some parameters of the typical closed hydrostatic guideway with four pads [8].

Parameters	Hydrostatic table			Total oil film clearance	External force
	l	*L*	*H*	$h_{01}+h_{02}$	F_0
Value	60.5 mm	125 mm	320 mm	40 μm	0 *N*
Parameters	Pad				Hydrostatic oil dynamic viscosity
	M	*m*	*W*	*w*	*η*
Value	60.5 mm	15 mm	50 mm	15 mm	0.065 Pa·s

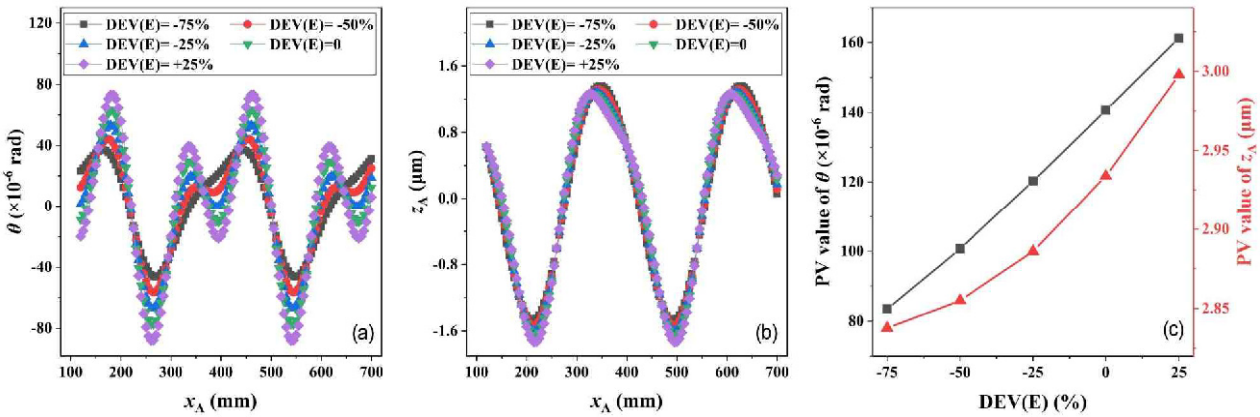

Fig. 5. Influence of amplitude deviation on motion accuracy: (a) Angular motion error; (b) linear motion error; (c) PV values of the two motion errors.

3. Influence of relative difference on motion accuracy

The relative difference between paired rails in typical closed hydrostatic guideway with four pads does refer to the relative deviations of guide rail profile error and the relative geometry position error. The former can be defined as

$$DEV(E)=(E_2-E_1)/E_1\times 100\%,$$
$$DEV(\lambda)=(\lambda_2-\lambda_1)/\lambda_1\times 100\%,\quad \delta(\varphi)=\varphi_2-\varphi_1 \tag{29}$$

where *DEV*(*E*) is amplitude deviation, *DEV*(*λ*) is wavelength deviation, and *δ*(*φ*) is phase deviation. The latter is defined as the parallelism error between paired guide rails, which is characterized by the angle *α* shown in Fig. 3. Some parameters of the typical closed hydrostatic guideway with four pads are given in Table 1. The other parameters are determined as follows. The key parameters of PM controller are 0.1×10^{-6} m^3/s of Q_0, 1.4 of K_r, and 5 MPa of P_s. The profile error components of rail 1 are 4 μm of E_1, 280 mm of λ_1, and 0 of φ_1. The stroke of the moving hydrostatic table is from 120 mm to 700 mm.

3.1 Relative deviations of guide rail profile error

In this section, the influence of three relative deviations on motion accuracy in closed hydrostatic guideway is studied without the consideration of the parallelism error. Thus, the mathematical functions of rail 1 and rail 2 can be explicitly expressed by Eqs. (10) and (11). First is the amplitude deviation *DEV*(*E*), and the values of *DEV*(*λ*) and *δ*(*φ*) are determined as -50 % and 0.3π, respectively. Fig. 5 shows the influence of amplitude deviation on motion accuracy. As shown in Fig. 5(a), from the horizontal point of view, with the moving of hydrostatic table along the positive direction of X_A axis, the peaks and valleys of the angular motion error curve occur periodically. However, from the vertical point of view, with the increase of *DEV*(*E*), those peaks and valleys become more noticeable and numerous. Fig. 5(b) depicts the variation of the linear motion error, which also is periodical. It can be observed that the linear motion error is rarely affected by *DEV*(*E*). Fig. 5(c) shows the PV values of the two motion errors, with the growth of *DEV*(*E*), both of those two PV values rise. Consequently, in order to improve the motion accuracy in closed hydrostatic guideway, one of the effective approaches is to reduce the guide rail profile error amplitude, such as scraping or lapping by the skilled workers [10, 12, 27].

Then is the wavelength deviation *DEV*(*λ*). Here, *DEV*(*E*) = -50 %, *δ*(*φ*) = 0.3π. Fig. 6 shows the influence of wavelength deviation on motion accuracy. As shown in Figs. 6(a) and (b), with the moving of hydrostatic table in the determined stroke, neither of the two motion errors fluctuates periodically, while the overall trends of those curves in Figs. 6(a) and (b) are similar, respectively. Take Fig. 6(a) as the instance, the peaks all occur at x_A≈400 mm and the valleys are seen at x_A≈260 mm and x_A≈550 mm. In addition, there is no significant regularity with the growth of *DEV*(*λ*). Fig. 6(c) shows the PV values of the two motion errors. With the increase of *DEV*(*λ*), the variation trends of those two PV values are not always the same with each other, which can be attributed to the design parameters of hydrostatic guideways. Zha et al. [10] has suggested that,

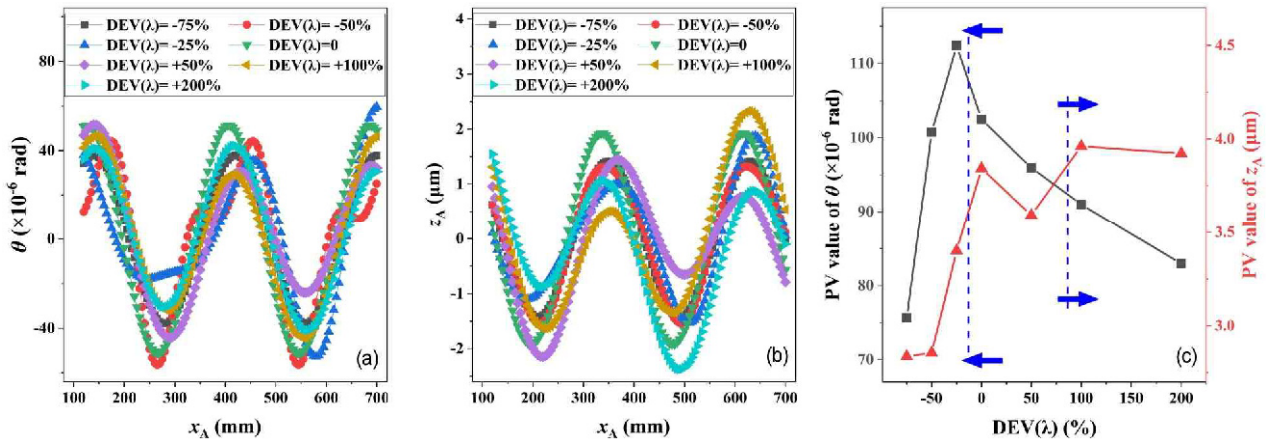

Fig. 6. Influence of wavelength deviation on motion accuracy: (a) Angular motion error; (b) linear motion error; (c) PV values of the two motion errors.

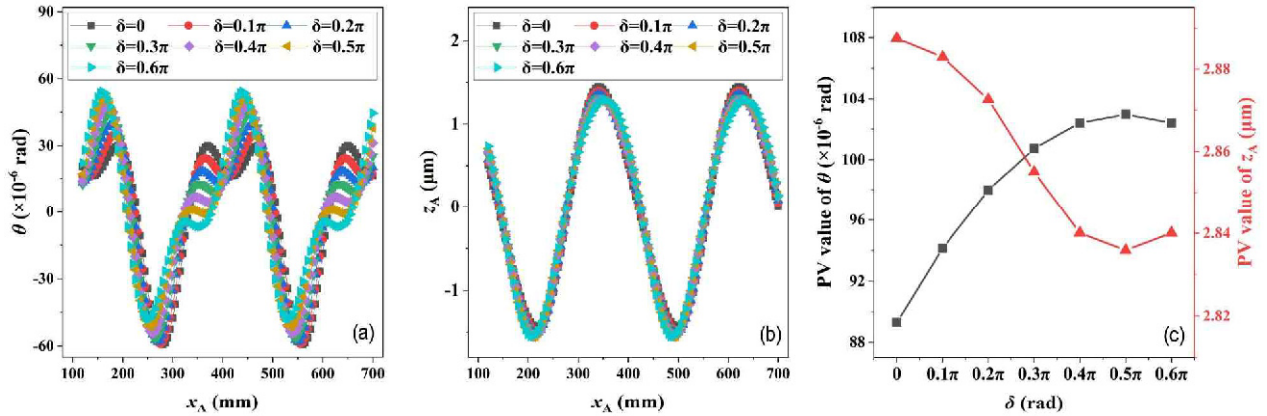

Fig. 7. Influence of phase deviation on motion accuracy: (a) Angular motion error; (b) linear motion error; (c) PV values of the two motion errors.

there can have two constants C_1 and C_2, when the ratio (l_λ) of pad center spacing (l) to guide rail profile error wavelength (λ) equal or lesser than C_1, keep λ unchanged, and the greater the pad center spacing (l), the higher the motion accuracy, whereas l_λ equal or larger than C_2, still keep λ invariant, the smaller the pad center spacing (l), the higher the motion accuracy. Indeed, this is equivalent to that, when $l_\lambda \le C_1$ and l is unchanged, the smaller the λ, the higher the motion accuracy, besides, when $l_\lambda \ge C_2$ and l is still invariant, the greater the λ, the higher the motion accuracy. From Fig. 6(c), it can be inferred that, before -25 % of $DEV(\lambda)$, the two motion errors reduce with the decrease of $DEV(\lambda)$, nevertheless, after +100 % of $DEV(\lambda)$, the greater the $DEV(\lambda)$, the smaller the two motion errors. Thus, those design parameters must be determined appropriately to accomplish the desired motion accuracy in hydrostatic guideways.

Last is the phase deviation $\delta(\varphi)$. Here, $DEV(\lambda) = DEV(E) = -50$ %. Fig. 7 shows the influence of phase deviation on motion accuracy. As depicted in Fig. 7(a), the angular motion error curve fluctuates periodically with the moving of hydrostatic table along the positive direction of X_A axis. Besides, with the rise of δ, the height difference between two adjacent peaks appears and becomes obvious gradually, simultaneously, the curve moves up and left. Fig. 7(b) shows the linear motion error curve, and it also changes periodically with the moving of hydrostatic table along the positive direction of X_A axis, but can be rarely affected by δ. Fig. 7(c) gives the PV values of the two motion errors, but they do perform the opposite trends with the increase of δ. Take the angular motion error as the example, when $\delta \le 0.5\pi$, the PV value increases nonlinearly with the growth of δ. At $\delta = 0.5\pi$, it reaches the maximum value. With the continuing increase of δ further, the PV value begins to slow down. It also can be observed from Fig. 7(c) that, the maximum change rate of angular motion error PV value is about 15.32 %, but that of the linear motion error PV value is around 1.79 % only. Accordingly, is it possible to exist the dominant motion error and the secondary motion error?

3.2 Parallelism error between paired guide rails

As mentioned in Sec. 2.2, there has $-\gamma = \beta = \alpha/2$, and the angle α is used to represent the parallelism error. Even though Eq. (28) gives the method to calculate h_a, the large amount of calculation is unavoidable, which is resulted from the implicit mathematical expression of guide rail profile error. In Sec. 3.1, take no account of the parallelism error, Eqs. (8) and (9) can be

transformed into Eqs. (11) and (10), respectively. So the mathematical functions of guide rail profile errors become explicit, and h_a is easy to be solved. If those mathematical functions in this section are not only explicit but also can characterize the parallelism error, then the amount of calculation will be reduced significantly and the influence of the parallelism error on motion accuracy still can be investigated. According to Ref. [2], these functions do exist and are given as

$$
\begin{aligned}
{}^{A}Z_1 = &-\frac{h_0}{2} - c_1 \sin\left[c_{11}\cdot\frac{2\pi}{\lambda_{11}}\cdot {}^{A}X\right] \\
&-b_1 \sin\left[b_{11}\cdot\frac{2\pi}{\lambda_{12}}\cdot {}^{A}X\right] - a_1\cdot {}^{A}X
\end{aligned} \tag{30}
$$

$$
\begin{aligned}
{}^{A}Z_2 = &\frac{h_0}{2} + c_2 \sin\left[c_{22}\cdot\frac{2\pi}{\lambda_{21}}\cdot {}^{A}X\right] \\
&+b_2 \sin\left[b_{22}\cdot\frac{2\pi}{\lambda_{22}}\cdot {}^{A}X\right] + a_2\cdot {}^{A}X
\end{aligned} \tag{31}
$$

Table 2. Values of those parameters involved in Eqs. (30) and (31).

Parameters	c_1	c_2	c_{11}	c_{22}
Value (m)	2.52×10^{-7}	5.04×10^{-7}	0.80	0.60
Parameters	b_1	b_2	b_{11}	b_{22}
Value (m)	3.36×10^{-6}	2.24×10^{-6}	1.10	1.10
Parameters	λ_{11}	λ_{12}	λ_{21}	λ_{22}
Value (m)	0.10	0.33	0.12	0.42

where ${}^{A}Z_1$ and ${}^{A}Z_2$ denote the explicit mathematical functions of rail 1 and rail 2, respectively. In addition, set a_1 to be equal to a_2, then there has $a_1 = a_2 = -\tan\alpha$, so α can be replaced by a_1 to represent the parallelism error. Table 2 shows the values of those parameters involved in Eqs. (30) and (31). Fig. 8 illustrates the quantitative relationship between a_1 and the parallelism error based on the data in Table 2. However, the value of h_0 in Fig. 8 is intended to set as 8 μm in order to clearly sketch the profiles and relative position of the paired rails. This is because the actual value of h_0 is in decimeter order of magnitude shown in Table 1. It also can be seen from Fig. 8 that, the positive value of a_1 corresponds to the positive flared shape of the paired rails, whereas the negative value of a_1 corresponds to the negative flared shape.

Note that, Eqs. (8) and (9) are slightly different with Eqs. (30) and (31). For instance, at one certain x_A coordinate, with the reduction of α, ${}^{A}Z_2(x_A)$ increases and ${}^{A}Z_1(x_A)$ decreases. However, to Eqs. (8) and (9), the change rates of ${}^{A}Z_1(x_A)$ and ${}^{A}Z_2(x_A)$ are unequal due to the effect from the different profile features of the paired rails, in contrast, to Eqs. (30) and (31), the change rates are equal because of $a_1{}^{A}X$ in Eq. (30) and $a_2{}^{A}X$ in Eq. (31). Therefore, in order to greatly reduce the amount of calculation, as well as eliminate the effect from the profile errors of paired guide rails, the only one variable a_1 in this section is selected to study the influence of parallelism error on motion accuracy just based on Eqs. (30) and (31).

Fig. 9 shows the influence of a_1 on motion accuracy. With the change of a_1, the fluctuations of two motion errors are not

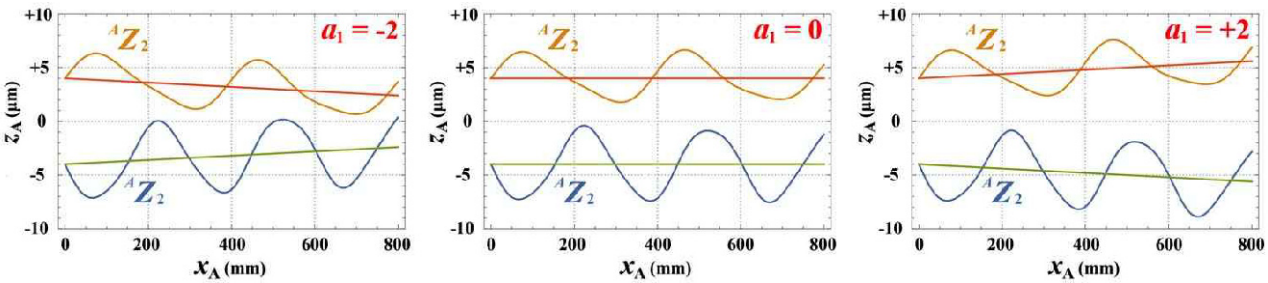

Fig. 8. Quantitative relationship between a_1 and the parallelism error based on the data in Table 2.

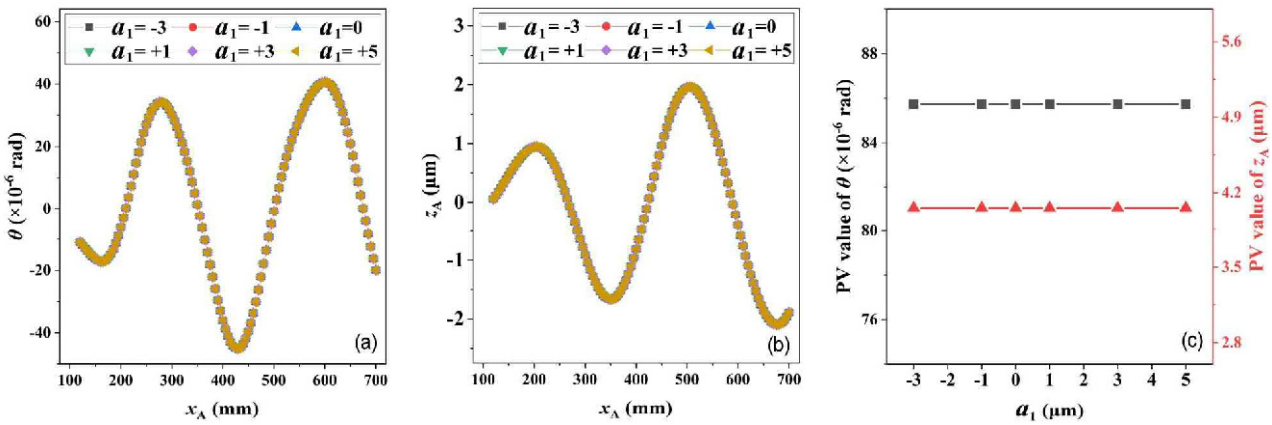

Fig. 9. Influence of a_1 on motion accuracy: (a) Angular motion error; (b) linear motion error; (c) PV values of the two motion errors.

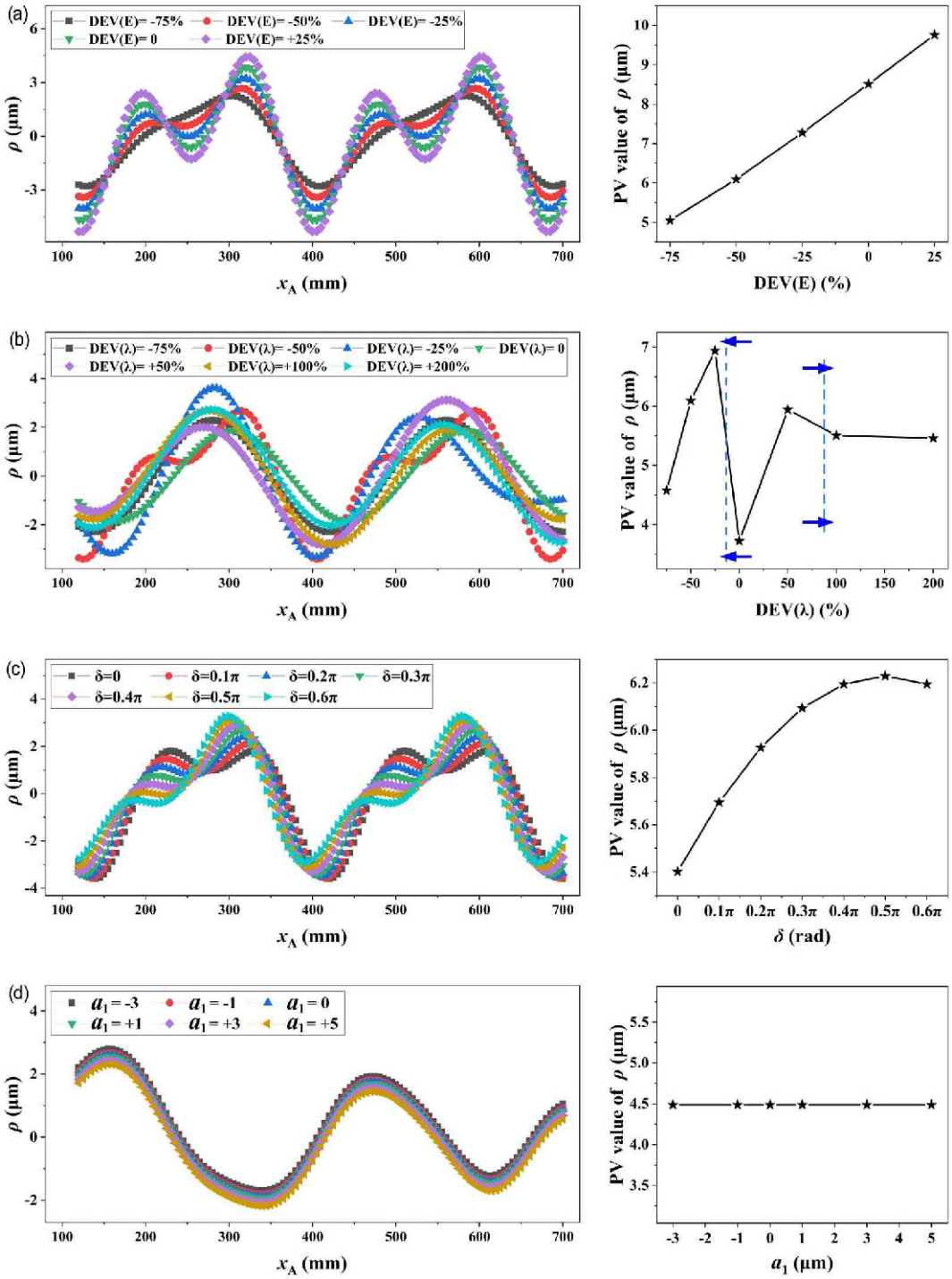

Fig. 10. Variation of ρ and the corresponding PV value: (a) DEV(E); (b) DEV(λ); (c) δ(φ); (d) the parameter a_1 representing the parallelism error.

affected at all, as shown in Figs. 9(a) and (b). Besides, it can be observed from Fig. 9(c) that the PV values of the two motion errors also are rarely influenced by a_1. So it seems that the motion accuracy cannot be effectively improved by reducing the parallelism error between paired guide rails. As mentioned above, with the variation of a_1, the change rates of ${}^{A}Z_1(x_A)$ and ${}^{A}Z_2(x_A)$ at one certain x_A coordinate are equal. In other words, the equal variations of the average oil film clearances on the two opposed pads (such as pad 1 and 2 or pad 3 and 4 shown in Fig. 2) may not have a significant effect on motion accuracy. It can be interpreted as that, the clearance does affect the stiffness of the guideways [2], while the stiffness almost does not result in the variation of motion errors [27]. Hence, the mechanisms affecting motion accuracy have to be analyzed next.

4. Discussion

Based on the analysis results above, it can be known that the relative difference between paired rails do has an effect on motion accuracy in closed hydrostatic guideways. Here, the mechanisms affecting motion accuracy are given further. Khim et al. [15] and Xue et al. [6] indicated that the motion errors were linked to the oil film reaction forces on the pads. According to Eqs. (24)-(27), the oil film reaction force is directly related to h_a. So the variation of h_a should be paid close attention to interpret the motion errors. Specifically, as shown in Table 1, Eqs. (19) and (20), it is $F_1 = F_2$ and $F_3 = F_4$ that always holds, so there will always be $h_{a1} = h_{a2}$ and $h_{a3} = h_{a4}$. Afterwards, the difference between the average film thicknesses of two adjacent pads (such as pad 1 and 3 or pad 2 and 4 shown in Fig. 2) is named as ρ, which is mathematically expressed as $\rho = h_{a1}(h_{a2})\text{-}h_{a3}(h_{a4})$. It may be very naturally inferred that, the greater the fluctuation of ρ, the larger the motion errors, and the poorer the motion accuracy.

Fig. 10 shows the variation of ρ and the corresponding PV value. The fluctuation of ρ can be observed easily, which is attributed to the two motion errors θ and z_A. Note that, the trajectory of any point on the hydrostatic table can be determined by those two motion errors [5, 10]. The influence of $DEV(E)$ on ρ can be seen from Fig. 10(a), and the variation of ρ is periodical, besides, with the growth of $DEV(E)$, the fluctuation of ρ becomes significant, and the corresponding PV value also rises, which just interprets the phenomenon presented in Fig. 5 that the greater the $DEV(E)$, the larger the two motion errors. Fig. 10(b) depicts the influence of $DEV(\lambda)$ on ρ. Within the determined stroke, the fluctuation of ρ does not exhibit the periodicity distinctly, however, it can be observed from the variation of PV value that, before -25 % of $DEV(\lambda)$, the smaller the $DEV(\lambda)$, the smaller the PV value, which corresponds to the decrease of the two motion errors shown in Fig. 6, while after +100 % of $DEV(\lambda)$, with the increase of $DEV(\lambda)$, the PV value reduces, which again corresponds to the decrease of the two motion errors shown in Fig. 6. The influence of $\delta(\varphi)$ on ρ is illustrated in Fig. 10(c), and ρ changes periodically. With the rise of $\delta(\varphi)$, the variation trend of PV value here is almost consistent with that of the angular motion error PV value shown in Fig. 7(c), so it can be confirmed that the dominant and secondary motion errors are θ and z_A, respectively. Lastly, Fig. 10(d) shows the influence of a_1 representing the parallelism error on ρ. The periodical variation of ρ is not significant. With the increase of a_1, the variation curve of ρ moves down slowly, but the corresponding PV value always be constant, which does account for that the two motion errors are not affected by a_1.

As depicted in Fig. 1(e), the X axis of UPG 80 contains three closed hydrostatic guideways, they are paired guide rails A & B, C & D, E & F, respectively. The structure consisting of paired guide rails A & B, pads A and B of HGS 1, pads A and B of HGS 3 shown in Fig. 1 can be equivalently seen as the typical closed hydrostatic guideway with four pads just shown in Fig. 2. Although the quasi-static analysis model for the closed hydrostatic guideway with four pads has been established, and the numerical results as well as the revealed mechanisms also are presented thoroughly, different pads and guideways still should be selected to verify the effectivity of the quasi-static analysis model so as to make our research become more convincing. Indeed, the research work on the effectivity of this analysis model for six HGSs (twelve pads) has already been verified by experimental data before, its modeling is similar but not quite the same with that proposed in this paper due to the structural differences between them. The verification of the quasi-static analysis model for the closed hydrostatic guideways with six HGSs (twelve pads) has been given in Appendix A.2, whereas the similar modeling will be no longer repeated. The good agreement between measured vertical straightness errors and computational results does verify the effectivity of the quasi-static analysis model.

5. Conclusions

In this paper, the development of quasi-static analysis model for the typical closed hydrostatic guideway with four pads is accomplished directly by incorporating the concept of pose, then the model is used to study the influence of relative difference between paired rails on motion accuracy. The analysis results suggest that the relative deviations of guide rail profile error, but not the parallelism error between paired guide rails, do have an effect on the motion accuracy significantly. The greater the amplitude deviation, the larger the motion errors. The influence of wavelength deviation on motion accuracy presents regularity within some intervals, before -25 % of $DEV(\lambda)$, the two motion errors reduce with the decrease of $DEV(\lambda)$, nevertheless, after +100 % of $DEV(\lambda)$, the greater the $DEV(\lambda)$, the smaller the two motion errors. The phase deviation mainly affects the angular motion error but not the linear motion error. Further, it has been known that the fluctuation of the difference between the average film thicknesses of two adjacent pads leads to the variation of the motion accuracy, and the greater the fluctuation, the larger the motion errors. The research work has provided theoretical references for the precision design of UPG 80 and also is applicable to the improvement of other hydrostatic guideways.

Acknowledgments

This work was financially supported by the National Science and Technology Major Project of the Ministry of Science and Technology of China (2017ZX04022001-207). We appreciate the invaluable expert comments and advice on the paper from all anonymous reviewers.

Nomenclature

L : Length of hydrostatic table

H : Width of hydrostatic table
B : Height of hydrostatic table
l : Center spacing between two adjacent pads
M : Length of pad
W : Width of pad
E_1 : Guide rail 1's profile error amplitude
λ_1 : Guide rail 1's profile error wavelength
φ_1 : Guide rail 1's profile error phase
E_2 : Guide rail 2's profile error amplitude
λ_2 : Guide rail 2's profile error wavelength
φ_2 : Guide rail 2's profile error phase
$\{A\}$: Reference coordinate system
$\{B\}$: Hydrostatic table coordinate system
$\{C\}$: Neutral plane coordinate systems of rail 1
$\{D\}$: Neutral plane coordinate systems of rail 2
h_0 : Sum of oil film clearance h_{01} and h_{02}
${}^{A}\boldsymbol{p}$: Description of point $\boldsymbol{p}$ on the curved profile in $\{A\}$
${}^{D}\boldsymbol{p}$: Description of point $\boldsymbol{p}$ on the curved profile in $\{D\}$
${}^{A}\boldsymbol{q}$: Description of point $\boldsymbol{q}$ on the hydrostatic table in $\{A\}$
${}^{B}\boldsymbol{q}$: Description of point $\boldsymbol{q}$ on the hydrostatic table in $\{B\}$
${}^{A}_{D}\boldsymbol{R}$: Rotation matrix (representing the orientation of $\{D\}$ relative to $\{A\}$)
${}^{A}_{B}\boldsymbol{R}$: Rotation matrix (representing the orientation of $\{B\}$ relative to $\{A\}$)
${}^{A}\boldsymbol{p}_{Do}$: Translation vector of $\{D\}$ relative to $\{A\}$
${}^{A}\boldsymbol{q}_{Bo}$: Translation vector of $\{B\}$ relative to $\{A\}$
F_0 : External force acting on the hydrostatic table
$F_1 \sim F_4$: The four oil film reaction forces
e : Arm of F_0
z_A : Linear motion error
θ : Angular motion error
i : Number of pad
j : Number of point in one pad plane
${}^{A}\boldsymbol{q}_{ij}$: Coordinates of the jth point in the ith pad plane in $\{A\}$
${}^{B}\boldsymbol{q}_{ij}$: Coordinates of the jth point in the ith pad plane in $\{B\}$
P_r : Hydrostatic pressure in the recess
A_e : Effective bearing area of the rectangle pad
Q : Flow rate corresponding to P_r
Q_0 : Flow rate for $P_r = 0$
K_r : Flow ratio of PM controller
P_s : Supply pressure
R : Flow resistance of the land
h : Nominal oil film thickness
h_a : Average oil film thickness
A_{land} : Projected area of land in the plane $O_A X_A Y_A$
$DEV(E)$: Amplitude deviation
$DEV(\lambda)$: Wavelength deviation
$\delta(\varphi)$: Phase deviation
α : Parallelism error between paired guide rails
η : Hydrostatic oil dynamic viscosity
l_λ : The ratio of l to λ
${}^{A}Z_1$: Explicit mathematical functions of rail 1
${}^{A}Z_2$: Explicit mathematical functions of rail 2
ρ : The difference between h_a of two adjacent pads
HGS : Hydrostatic guide shoe

References

[1] Z. Wang, Y. Liu and F. Wang, Rapid calculation method for estimating static and dynamic performances of closed hydrostatic guideways, *Industrial Lubrication and Tribology*, 69 (6) (2017) 1040-1048.

[2] J. Hwang et al., A three-probe system for measuring the parallelism and straightness of a pair of rails for ultra-precision guideways, *International J. of Machine Tools and Manufacture*, 47 (7-8) (2007) 1053-1058.

[3] Y. Kang et al., Modified predictions of restriction coefficient and flow resistance for membrane-type restrictors in hydrostatic bearing by using regression, *Tribology International*, 40 (9) (2007) 1369-1380.

[4] M. Zhao et al., Hydrostatic pressure calculation and optimization for design of beam & slide-rest guideways in heavy duty CNC vertical turning mill, *Chinese J. of Mechanical Engineering*, 20 (5) (2007) 16-22.

[5] J. Zha, F. Xue and Y. Chen, Straightness error modeling and compensation for gantry type open hydrostatic guideways in grinding machine, *International J. of Machine Tools and Manufacture*, 112 (2017) 1-6.

[6] F. Xue et al., Research on error averaging effect of hydrostatic guideways, *Precision Engineering*, 36 (1) (2012) 84-90.

[7] S. Xiang and J. Yang, Error map construction and compensation of a NC lathe under thermal and load effects, *The International J. of Advanced Manufacturing Technology*, 79 (1-4) (2015) 645-655.

[8] Z. Wang et al., Prediction of the effect of speed on motion errors in hydrostatic guideways, *International J. of Machine Tools and Manufacture*, 64 (2013) 78-84.

[9] P. Zhang et al., Influence of geometric errors of guide rails and table on motion errors of hydrostatic guideways under quasi-static condition, *International J. of Machine Tools and Manufacture*, 125 (2018) 55-67.

[10] J. Zha et al., Motion straightness of hydrostatic guideways considering the ratio of pad center spacing to guide rail profile error wavelength, *The International J. of Advanced Manufacturing Technology*, 82 (9-12) (2016) 2065-2073.

[11] F. Xue and W. Zhao, Influencing factors on error averaging effect of hydrostatic guideways, *J. of Xi'an Jiaotong University*, 44 (11) (2010) 33-36 (in Chinese).

[12] E. Shamoto, C. H. Park and T. Moriwaki, Analysis and improvement of motion accuracy of hydrostatic feed table, *CIRP Annals*, 50 (1) (2001) 285-290.

[13] S. Y. Jeon and K. H. Kim, A fluid film model for finite element analysis of structures with linear hydrostatic bearings, *Proceedings of the Institution of Mechanical Engineers, Part C: J. of Mechanical Engineering Science*, 218 (3) (2004) 309-316.

[14] E. Qi et al., A method for predicting hydrostatic guide error averaging effects based on three-dimensional profile error, *Tribology International*, 95 (2016) 279-289.

[15] G. Khim, J. S. Oh and C. H. Park, Analysis of 5-DOF motion errors influenced by the guide rails of an aerostatic linear motion stage, *International J. of Precision Engineering and Manu-*

facturing, 15 (2) (2014) 283-290.
[16] H. Hong and Y. Yin, Ontology-based conceptual design for ultra-precision hydrostatic guideways with human-machine interaction, *J. of Industrial Information Integration*, 2 (2016) 11-18.
[17] Y. Altintas et al., Virtual machine tool, *CIRP Annals*, 54 (2) (2005) 115-138.
[18] J. S. Oh et al., Accuracy simulation of the precision linear motion systems, *J. of the Korean Society for Precision Engineering*, 28 (3) (2011) 275-284.
[19] G. H. Kim, J. A. Han and S. K. Lee, Motion error estimation of slide table on the consideration of guide parallelism and pad deflection, *International J. of Precision Engineering and Manufacturing*, 15 (9) (2014) 1935-1946.
[20] N. R. Kane, J. Sihler and A. H. Slocum, A hydrostatic rotary bearing with angled surface self-compensation, *Precision Engineering*, 27 (2) (2003) 125-139.
[21] P. Corke, *Robotics, Vision and Control: Fundamental Algorithms in MATLAB*, 1st ed., Publishing House of Electronics Industry, Beijing, China (2016).
[22] D. Gao et al., Research on the influence of PM controller parameters on the performance of hydrostatic slide for NC machine tool, *J. of Mechanical Engineering*, 47 (18) (2011) 186-194 (in Chinese).
[23] D. Gao, D. Zheng and Z. Zhang, Theoretical analysis and numerical simulation of the static and dynamic characteristics of hydrostatic guides based on progressive mengen flow controller, *Chinese J. of Mechanical Engineering*, 23 (6) (2010) 709-716.
[24] S. Yang et al., Hydrostatic worktable performance of an ultra-precision optical aspheric machine tool, *Procedia CIRP*, 27 (2015) 187-191.
[25] L. Chen et al., Influence of parameters of PM controller on vibration performance of liquid hydrostatic guide-way system, *Noise & Vibration Worldwide*, 49 (4) (2018) 140-146.
[26] W. B. Rowe, *Hydrostatic and Hybrid Bearing Design*, 1st ed., Butterworth, London, UK (1983).
[27] G. Khim et al., Prediction and compensation of motion accuracy in a linear motion bearing table, *Precision Engineering*, 35 (3) (2011) 393-399.

Appendix

A.1 Coordinate transformation between {*A*} and {*B*}

Table A.1. The corresponding relationship between ${}^{B}\boldsymbol{q}_{ij}$ and ${}^{A}\boldsymbol{q}_{ij}$.

(i, j)	**(1, 0)**	**(1, 1)**	**(1, 2)**
${}^{B}\boldsymbol{q}_{ij}$	$\left[-\frac{l}{2} \quad 0 \quad -\frac{H}{2}\right]^{\mathrm{T}}$	$\left[-\frac{l}{2}-\frac{M}{2} \quad -\frac{W}{2} \quad -\frac{H}{2}\right]^{\mathrm{T}}$	$\left[-\frac{l}{2}+\frac{M}{2} \quad -\frac{W}{2} \quad -\frac{H}{2}\right]^{\mathrm{T}}$
${}^{A}\boldsymbol{q}_{ij}$	$\begin{bmatrix} x_{\mathrm{A}}-\frac{l}{2}\cos\theta-\frac{H}{2}\sin\theta \\ 0 \\ z_{\mathrm{A}}-\frac{H}{2}\cos\theta+\frac{l}{2}\sin\theta \end{bmatrix}$	$\begin{bmatrix} x_{\mathrm{A}}+\left(-\frac{l}{2}-\frac{M}{2}\right)\cos\theta-\frac{H}{2}\sin\theta \\ -\frac{W}{2} \\ z_{\mathrm{A}}-\frac{H}{2}\cos\theta-\left(-\frac{l}{2}-\frac{M}{2}\right)\sin\theta \end{bmatrix}$	$\begin{bmatrix} x_{\mathrm{A}}+\left(-\frac{l}{2}+\frac{M}{2}\right)\cos\theta-\frac{H}{2}\sin\theta \\ -\frac{W}{2} \\ z_{\mathrm{A}}-\frac{H}{2}\cos\theta-\left(-\frac{l}{2}+\frac{M}{2}\right)\sin\theta \end{bmatrix}$
(i, j)	**(1, 3)**	**(1, 4)**	**(1, 5)**
${}^{B}\boldsymbol{q}_{ij}$	$\left[-\frac{l}{2}+\frac{M}{2} \quad \frac{W}{2} \quad -\frac{H}{2}\right]^{\mathrm{T}}$	$\left[-\frac{l}{2}-\frac{M}{2} \quad \frac{W}{2} \quad -\frac{H}{2}\right]^{\mathrm{T}}$	$\left[-\frac{l}{2}-\frac{M}{2}+m \quad -\frac{W}{2}+w \quad -\frac{H}{2}\right]^{\mathrm{T}}$
${}^{A}\boldsymbol{q}_{ij}$	$\begin{bmatrix} x_{\mathrm{A}}+\left(-\frac{l}{2}+\frac{M}{2}\right)\cos\theta-\frac{H}{2}\sin\theta \\ \frac{W}{2} \\ z_{\mathrm{A}}-\frac{H}{2}\cos\theta-\left(-\frac{l}{2}+\frac{M}{2}\right)\sin\theta \end{bmatrix}$	$\begin{bmatrix} x_{\mathrm{A}}+\left(-\frac{l}{2}-\frac{M}{2}\right)\cos\theta-\frac{H}{2}\sin\theta \\ \frac{W}{2} \\ z_{\mathrm{A}}-\frac{H}{2}\cos\theta-\left(-\frac{l}{2}-\frac{M}{2}\right)\sin\theta \end{bmatrix}$	$\begin{bmatrix} x_{\mathrm{A}}+\left(-\frac{l}{2}+m-\frac{M}{2}\right)\cos\theta-\frac{H}{2}\sin\theta \\ W-\frac{w}{2} \\ z_{\mathrm{A}}-\frac{H}{2}\cos\theta-\left(-\frac{l}{2}+m-\frac{M}{2}\right)\sin\theta \end{bmatrix}$
(i, j)	**(1, 6)**	**(1, 7)**	**(1, 8)**
${}^{B}\boldsymbol{q}_{ij}$	$\left[-\frac{l}{2}+\frac{M}{2}-m \quad -\frac{W}{2}+w \quad -\frac{H}{2}\right]^{\mathrm{T}}$	$\left[-\frac{l}{2}+\frac{M}{2}-m \quad \frac{W}{2}-w \quad -\frac{H}{2}\right]^{\mathrm{T}}$	$\left[-\frac{l}{2}-\frac{M}{2}+m \quad \frac{W}{2}-w \quad -\frac{H}{2}\right]^{\mathrm{T}}$
${}^{A}\boldsymbol{q}_{ij}$	$\begin{bmatrix} x_{\mathrm{A}}+\left(-\frac{l}{2}-m+\frac{M}{2}\right)\cos\theta-\frac{H}{2}\sin\theta \\ W-\frac{w}{2} \\ z_{\mathrm{A}}-\frac{H}{2}\cos\theta-\left(-\frac{l}{2}-m+\frac{M}{2}\right)\sin\theta \end{bmatrix}$	$\begin{bmatrix} x_{\mathrm{A}}+\left(-\frac{l}{2}-m+\frac{M}{2}\right)\cos\theta-\frac{H}{2}\sin\theta \\ -W+\frac{w}{2} \\ z_{\mathrm{A}}-\frac{H}{2}\cos\theta-\left(-\frac{l}{2}+m-\frac{M}{2}\right)\sin\theta \end{bmatrix}$	$\begin{bmatrix} x_{\mathrm{A}}+\left(-\frac{l}{2}+m-\frac{M}{2}\right)\cos\theta-\frac{H}{2}\sin\theta \\ -W+\frac{w}{2} \\ z_{\mathrm{A}}-\frac{H}{2}\cos\theta-\left(-\frac{l}{2}+m-\frac{M}{2}\right)\sin\theta \end{bmatrix}$

Table A.1. (continued)

(i, j)	**(2, 0)**	**(2, 1)**	**(2, 2)**
${}^{B}\boldsymbol{q}_{ij}$	$\left[-\frac{l}{2} \quad 0 \quad \frac{H}{2}\right]^{\mathrm{T}}$	$\left[-\frac{l}{2}-\frac{M}{2} \quad -\frac{W}{2} \quad \frac{H}{2}\right]^{\mathrm{T}}$	$\left[-\frac{l}{2}+\frac{M}{2} \quad -\frac{W}{2} \quad \frac{H}{2}\right]^{\mathrm{T}}$
${}^{A}\boldsymbol{q}_{ij}$	$\begin{bmatrix} x_{\mathrm{A}}-\frac{l}{2}\cos\theta+\frac{H}{2}\sin\theta \\ 0 \\ z_{\mathrm{A}}+\frac{H}{2}\cos\theta+\frac{l}{2}\sin\theta \end{bmatrix}$	$\begin{bmatrix} x_{\mathrm{A}}+\left(-\frac{l}{2}-\frac{M}{2}\right)\cos\theta+\frac{H}{2}\sin\theta \\ -\frac{W}{2} \\ z_{\mathrm{A}}+\frac{H}{2}\cos\theta-\left(-\frac{l}{2}-\frac{M}{2}\right)\sin\theta \end{bmatrix}$	$\begin{bmatrix} x_{\mathrm{A}}+\left(-\frac{l}{2}+\frac{M}{2}\right)\cos\theta+\frac{H}{2}\sin\theta \\ -\frac{W}{2} \\ z_{\mathrm{A}}+\frac{H}{2}\cos\theta-\left(-\frac{l}{2}+\frac{M}{2}\right)\sin\theta \end{bmatrix}$
(i, j)	**(2, 3)**	**(2, 4)**	**(2, 5)**
${}^{B}\boldsymbol{q}_{ij}$	$\left[-\frac{l}{2}+\frac{M}{2} \quad \frac{W}{2} \quad \frac{H}{2}\right]^{\mathrm{T}}$	$\left[-\frac{l}{2}-\frac{M}{2} \quad \frac{W}{2} \quad \frac{H}{2}\right]^{\mathrm{T}}$	$\left[-\frac{l}{2}-\frac{M}{2}+m \quad -\frac{W}{2}+w \quad \frac{H}{2}\right]^{\mathrm{T}}$
${}^{A}\boldsymbol{q}_{ij}$	$\begin{bmatrix} x_{\mathrm{A}}+\left(-\frac{l}{2}+\frac{M}{2}\right)\cos\theta+\frac{H}{2}\sin\theta \\ \frac{W}{2} \\ z_{\mathrm{A}}+\frac{H}{2}\cos\theta-\left(-\frac{l}{2}+\frac{M}{2}\right)\sin\theta \end{bmatrix}$	$\begin{bmatrix} x_{\mathrm{A}}+\left(-\frac{l}{2}-\frac{M}{2}\right)\cos\theta+\frac{H}{2}\sin\theta \\ \frac{W}{2} \\ z_{\mathrm{A}}+\frac{H}{2}\cos\theta-\left(-\frac{l}{2}-\frac{M}{2}\right)\sin\theta \end{bmatrix}$	$\begin{bmatrix} x_{\mathrm{A}}+\left(-\frac{l}{2}+m-\frac{M}{2}\right)\cos\theta+\frac{H}{2}\sin\theta \\ W-\frac{w}{2} \\ z_{\mathrm{A}}+\frac{H}{2}\cos\theta-\left(-\frac{l}{2}+m-\frac{M}{2}\right)\sin\theta \end{bmatrix}$
(i, j)	**(2, 6)**	**(2, 7)**	**(2, 8)**
${}^{B}\boldsymbol{q}_{ij}$	$\left[-\frac{l}{2}+\frac{M}{2}-m \quad -\frac{W}{2}+w \quad \frac{H}{2}\right]^{\mathrm{T}}$	$\left[-\frac{l}{2}+\frac{M}{2}-m \quad \frac{W}{2}-w \quad \frac{H}{2}\right]^{\mathrm{T}}$	$\left[-\frac{l}{2}-\frac{M}{2}+m \quad \frac{W}{2}-w \quad \frac{H}{2}\right]^{\mathrm{T}}$
${}^{A}\boldsymbol{q}_{ij}$	$\begin{bmatrix} x_{\mathrm{A}}+\left(-\frac{l}{2}-m+\frac{M}{2}\right)\cos\theta+\frac{H}{2}\sin\theta \\ W-\frac{w}{2} \\ z_{\mathrm{A}}+\frac{H}{2}\cos\theta-\left(-\frac{l}{2}-m+\frac{M}{2}\right)\sin\theta \end{bmatrix}$	$\begin{bmatrix} x_{\mathrm{A}}+\left(-\frac{l}{2}-m+\frac{M}{2}\right)\cos\theta+\frac{H}{2}\sin\theta \\ -W+\frac{w}{2} \\ z_{\mathrm{A}}+\frac{H}{2}\cos\theta-\left(-\frac{l}{2}-m+\frac{M}{2}\right)\sin\theta \end{bmatrix}$	$\begin{bmatrix} x_{\mathrm{A}}+\left(-\frac{l}{2}+m-\frac{M}{2}\right)\cos\theta+\frac{H}{2}\sin\theta \\ -W+\frac{w}{2} \\ z_{\mathrm{A}}+\frac{H}{2}\cos\theta-\left(-\frac{l}{2}+m-\frac{M}{2}\right)\sin\theta \end{bmatrix}$
(i, j)	**(3, 0)**	**(3, 1)**	**(3, 2)**
${}^{B}\boldsymbol{q}_{ij}$	$\left[\frac{l}{2} \quad 0 \quad -\frac{H}{2}\right]^{\mathrm{T}}$	$\left[\frac{l}{2}-\frac{M}{2} \quad -\frac{W}{2} \quad -\frac{H}{2}\right]^{\mathrm{T}}$	$\left[\frac{l}{2}+\frac{M}{2} \quad -\frac{W}{2} \quad -\frac{H}{2}\right]^{\mathrm{T}}$
${}^{A}\boldsymbol{q}_{ij}$	$\begin{bmatrix} x_{\mathrm{A}}+\frac{l}{2}\cos\theta-\frac{H}{2}\sin\theta \\ 0 \\ z_{\mathrm{A}}-\frac{H}{2}\cos\theta-\frac{l}{2}\sin\theta \end{bmatrix}$	$\begin{bmatrix} x_{\mathrm{A}}+\left(\frac{l}{2}-\frac{M}{2}\right)\cos\theta-\frac{H}{2}\sin\theta \\ -\frac{W}{2} \\ z_{\mathrm{A}}-\frac{H}{2}\cos\theta-\left(\frac{l}{2}-\frac{M}{2}\right)\sin\theta \end{bmatrix}$	$\begin{bmatrix} x_{\mathrm{A}}+\left(\frac{l}{2}+\frac{M}{2}\right)\cos\theta-\frac{H}{2}\sin\theta \\ -\frac{W}{2} \\ z_{\mathrm{A}}-\frac{H}{2}\cos\theta-\left(\frac{l}{2}+\frac{M}{2}\right)\sin\theta \end{bmatrix}$
(i, j)	**(3, 3)**	**(3, 4)**	**(3, 5)**
${}^{B}\boldsymbol{q}_{ij}$	$\left[\frac{l}{2}+\frac{M}{2} \quad \frac{W}{2} \quad -\frac{H}{2}\right]^{\mathrm{T}}$	$\left[\frac{l}{2}-\frac{M}{2} \quad \frac{W}{2} \quad -\frac{H}{2}\right]^{\mathrm{T}}$	$\left[\frac{l}{2}-\frac{M}{2}+m \quad -\frac{W}{2}+w \quad -\frac{H}{2}\right]^{\mathrm{T}}$
${}^{A}\boldsymbol{q}_{ij}$	$\begin{bmatrix} x_{\mathrm{A}}+\left(\frac{l}{2}+\frac{M}{2}\right)\cos\theta-\frac{H}{2}\sin\theta \\ \frac{W}{2} \\ z_{\mathrm{A}}-\frac{H}{2}\cos\theta-\left(\frac{l}{2}+\frac{M}{2}\right)\sin\theta \end{bmatrix}$	$\begin{bmatrix} x_{\mathrm{A}}+\left(\frac{l}{2}-\frac{M}{2}\right)\cos\theta-\frac{H}{2}\sin\theta \\ \frac{W}{2} \\ z_{\mathrm{A}}-\frac{H}{2}\cos\theta-\left(\frac{l}{2}-\frac{M}{2}\right)\sin\theta \end{bmatrix}$	$\begin{bmatrix} x_{\mathrm{A}}+\left(\frac{l}{2}+m-\frac{M}{2}\right)\cos\theta-\frac{H}{2}\sin\theta \\ W-\frac{w}{2} \\ z_{\mathrm{A}}-\frac{H}{2}\cos\theta-\left(\frac{l}{2}+m-\frac{M}{2}\right)\sin\theta \end{bmatrix}$
(i, j)	**(3, 6)**	**(3, 7)**	**(3, 8)**
${}^{B}\boldsymbol{q}_{ij}$	$\left[\frac{l}{2}+\frac{M}{2}-m \quad -\frac{W}{2}+w \quad -\frac{H}{2}\right]^{\mathrm{T}}$	$\left[\frac{l}{2}+\frac{M}{2}-m \quad \frac{W}{2}-w \quad -\frac{H}{2}\right]^{\mathrm{T}}$	$\left[\frac{l}{2}-\frac{M}{2}+m \quad \frac{W}{2}-w \quad -\frac{H}{2}\right]^{\mathrm{T}}$

Table A.1. (continued)

${}^{A}\boldsymbol{q}_{ij}$	$\begin{bmatrix} x_A+\left(\frac{l}{2}-m+\frac{M}{2}\right)\cos\theta-\frac{H}{2}\sin\theta \\ W-\frac{w}{2} \\ z_A-\frac{H}{2}\cos\theta-\left(\frac{l}{2}-m+\frac{M}{2}\right)\sin\theta \end{bmatrix}$	$\begin{bmatrix} x_A+\left(\frac{l}{2}-m+\frac{M}{2}\right)\cos\theta-\frac{H}{2}\sin\theta \\ -W+\frac{w}{2} \\ z_A-\frac{H}{2}\cos\theta-\left(\frac{l}{2}-m+\frac{M}{2}\right)\sin\theta \end{bmatrix}$	$\begin{bmatrix} x_A+\left(\frac{l}{2}+m-\frac{M}{2}\right)\cos\theta-\frac{H}{2}\sin\theta \\ -W+\frac{w}{2} \\ z_A-\frac{H}{2}\cos\theta-\left(\frac{l}{2}+m-\frac{M}{2}\right)\sin\theta \end{bmatrix}$
(i, j)	**(4, 0)**	**(4, 1)**	**(4, 2)**
${}^{B}\boldsymbol{q}_{ij}$	$\begin{bmatrix} \frac{l}{2} & 0 & \frac{H}{2} \end{bmatrix}^{\mathrm{T}}$	$\begin{bmatrix} \frac{l}{2}-\frac{M}{2} & -\frac{W}{2} & \frac{H}{2} \end{bmatrix}^{\mathrm{T}}$	$\begin{bmatrix} \frac{l}{2}+\frac{M}{2} & -\frac{W}{2} & \frac{H}{2} \end{bmatrix}^{\mathrm{T}}$
${}^{A}\boldsymbol{q}_{ij}$	$\begin{bmatrix} x_A+\frac{l}{2}\cos\theta+\frac{H}{2}\sin\theta \\ 0 \\ z_A+\frac{H}{2}\cos\theta-\frac{l}{2}\sin\theta \end{bmatrix}$	$\begin{bmatrix} x_A+\left(\frac{l}{2}-\frac{M}{2}\right)\cos\theta+\frac{H}{2}\sin\theta \\ -\frac{W}{2} \\ z_A+\frac{H}{2}\cos\theta-\left(\frac{l}{2}-\frac{M}{2}\right)\sin\theta \end{bmatrix}$	$\begin{bmatrix} x_A+\left(\frac{l}{2}+\frac{M}{2}\right)\cos\theta+\frac{H}{2}\sin\theta \\ -\frac{W}{2} \\ z_A+\frac{H}{2}\cos\theta-\left(\frac{l}{2}+\frac{M}{2}\right)\sin\theta \end{bmatrix}$
(i, j)	**(4, 3)**	**(4, 4)**	**(4, 5)**
${}^{B}\boldsymbol{q}_{ij}$	$\begin{bmatrix} \frac{l}{2}+\frac{M}{2} & \frac{W}{2} & \frac{H}{2} \end{bmatrix}^{\mathrm{T}}$	$\begin{bmatrix} \frac{l}{2}-\frac{M}{2} & \frac{W}{2} & \frac{H}{2} \end{bmatrix}^{\mathrm{T}}$	$\begin{bmatrix} \frac{l}{2}-\frac{M}{2}+m & -\frac{W}{2}+w & \frac{H}{2} \end{bmatrix}^{\mathrm{T}}$
${}^{A}\boldsymbol{q}_{ij}$	$\begin{bmatrix} x_A+\left(\frac{l}{2}+\frac{M}{2}\right)\cos\theta+\frac{H}{2}\sin\theta \\ \frac{W}{2} \\ z_A+\frac{H}{2}\cos\theta-\left(\frac{l}{2}+\frac{M}{2}\right)\sin\theta \end{bmatrix}$	$\begin{bmatrix} x_A+\left(\frac{l}{2}-\frac{M}{2}\right)\cos\theta+\frac{H}{2}\sin\theta \\ \frac{W}{2} \\ z_A+\frac{H}{2}\cos\theta-\left(\frac{l}{2}-\frac{M}{2}\right)\sin\theta \end{bmatrix}$	$\begin{bmatrix} x_A+\left(\frac{l}{2}+m-\frac{M}{2}\right)\cos\theta+\frac{H}{2}\sin\theta \\ W-\frac{w}{2} \\ z_A+\frac{H}{2}\cos\theta-\left(\frac{l}{2}+m-\frac{M}{2}\right)\sin\theta \end{bmatrix}$
(i, j)	**(4, 6)**	**(4, 7)**	**(4, 8)**
${}^{B}\boldsymbol{q}_{ij}$	$\begin{bmatrix} \frac{l}{2}+\frac{M}{2}-m & -\frac{W}{2}+w & \frac{H}{2} \end{bmatrix}^{\mathrm{T}}$	$\begin{bmatrix} \frac{l}{2}+\frac{M}{2}-m & \frac{W}{2}-w & \frac{H}{2} \end{bmatrix}^{\mathrm{T}}$	$\begin{bmatrix} \frac{l}{2}-\frac{M}{2}+m & \frac{W}{2}-w & \frac{H}{2} \end{bmatrix}^{\mathrm{T}}$
${}^{A}\boldsymbol{q}_{ij}$	$\begin{bmatrix} x_A+\left(\frac{l}{2}-m+\frac{M}{2}\right)\cos\theta+\frac{H}{2}\sin\theta \\ W-\frac{w}{2} \\ z_A+\frac{H}{2}\cos\theta-\left(\frac{l}{2}-m+\frac{M}{2}\right)\sin\theta \end{bmatrix}$	$\begin{bmatrix} x_A+\left(\frac{l}{2}-m+\frac{M}{2}\right)\cos\theta+\frac{H}{2}\sin\theta \\ -W+\frac{w}{2} \\ z_A+\frac{H}{2}\cos\theta-\left(\frac{l}{2}-m+\frac{M}{2}\right)\sin\theta \end{bmatrix}$	$\begin{bmatrix} x_A+\left(\frac{l}{2}+m-\frac{M}{2}\right)\cos\theta+\frac{H}{2}\sin\theta \\ -W+\frac{w}{2} \\ z_A+\frac{H}{2}\cos\theta-\left(\frac{l}{2}+m-\frac{M}{2}\right)\sin\theta \end{bmatrix}$

A.2 Experimental verification of the quasi-static analysis model

The closed hydrostatic guideways with six HGSs does refer to the structure of paired guide rails C & D, E & F, and all of the pads (except for pads A & B of HGS 1, pads A & B of HGS 3) shown in Fig. 1, thus, six HGSs mean twelve pads here.

The lengths of guide rails C, D, E and F depicted in Fig. 1 all are 3 m. As part of the bed, these guide rails are manufactured by horizontal surface grinding in the same grinding machine, which can result in the similar profile features. Note that, there is no scraping or lapping by the skilled workers. The profile errors of these guide rails could be measured and mathematically fitted as

$$Z_{\text{rail C}} = Z_{\text{rail E}} = 14\times10^{-6}\sin\left(\frac{2\pi\cdot X}{3.106\times10^{-6}}-0.14\pi\right) \quad \text{(A.1)}$$

$$Z_{\text{rail D}} = Z_{\text{rail F}} = 10\times10^{-6}\sin\left(\frac{2\pi\cdot X}{3.106\times10^{-6}}-0.14\pi\right) \quad \text{(A.2)}$$

It is noticed that, $Z_{\text{rail C}} = Z_{\text{rail E}}$ and $Z_{\text{rail D}} = Z_{\text{rail F}}$, afterwards, those six pads next to guide rails C and E are all connected by the same six fixed restrictors, but the other six pads next to guide rails D and F are all connected by the same six PM flow controllers, hence, the closed hydrostatic guideways with six HGSs above can be simplified as the closed hydrostatic guideway with six pads (three HGSs) futher, as observed from Fig. A.1. The pads E4 & F4, E5 & F5, E6 & F6 marked in Fig. A.1 correspond to the pads E & F of HGS 4, HGS 5, HGS 6 in Fig. 1, respectively. Therefore, the quasi-static analysis models for the closed hydrostatic guideway with six pads shown in Fig. A.1 and four pads shown in Fig. 2 both are 2-DOF models related to the angular and linear motion errors. The stroke of the moving hydrostatic table with six pads shown in Fig. A.1 is from 1650 mm to 2450 mm based on the reference coordinate system $\{A_{0B}\}$, which also can be expressed correspondingly as that the hydrostatic table with twelve pads shown in Fig. 1 slides from -200 mm to -1000 mm along the X axis of UPG 80 (its full stroke is from 0 mm to -1400 mm).

Table A.2. Parameters of calculation and experiments.

Parameters	Hydrostatic table with six pads			Total oil film clearance	Gravity of table
	l_{0B}	L_{0B}	H_{0B}	h_{0B} - H_{0B}	G
Value	550 mm	1300 mm	50 mm	50 μm	15288 N
Parameters	Pad E4 ~ Pad E6				Hydrostatic oil dynamic viscosity
	M_2	m_2	W_2	w_2	η
Value	200 mm	12 mm	43 mm	12 mm	0.1214 Pa·s
Parameters	Pad F4 ~ Pad F6				Room temperature
	M_1	m_1	W_1	w_1	T
Value	200 mm	12 mm	75 mm	12 mm	20℃
Parameters	PM flow controllers			Supply pressure	Flow resistance of fixed restrictors
	Q_0		K_r	P_s	R_{fixed}
Value	0.3667×10^{-6} m^3/s		2.8	3.2 MPa	2.2857×10^{12}

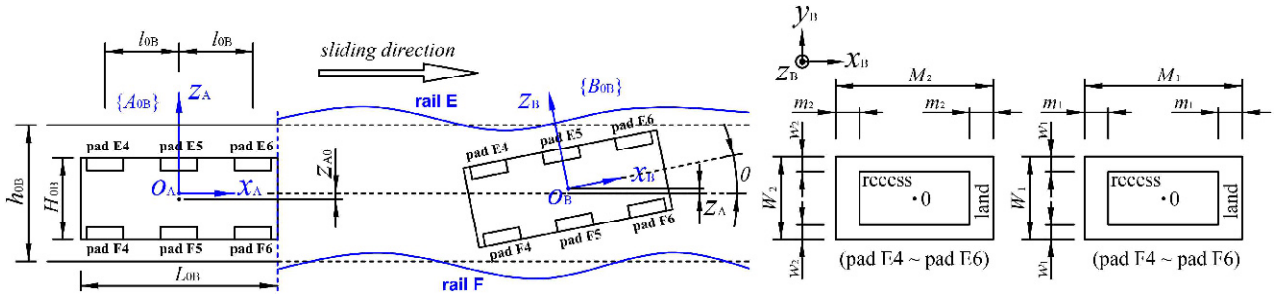

Fig. A.1. Closed hydrostatic guideway with six pads.

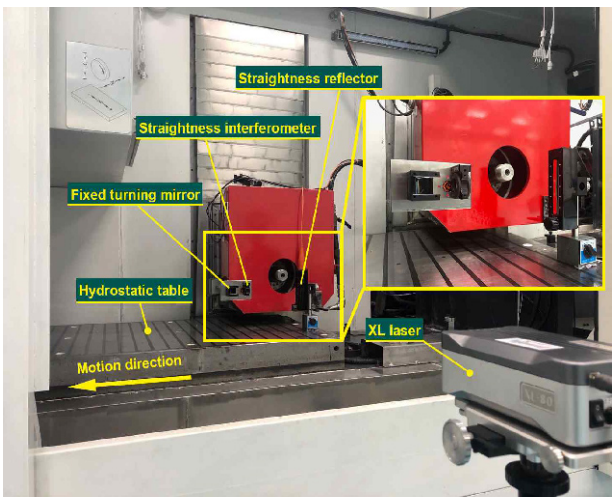

Fig. A.2. Measurement of the vertical straightness error by the Renishaw XL80.

The other parameters involved in calculation and experiments has been illustrated in Table A.2. Fig. A.2 shows the measurement of the vertical straightness error by the Renishaw XL80 Laser interferometer. The location of the straightness reflector in $\{B_{0B}\}$ is drawn simply but clearly in Fig. A.3.

Lastly, the vertical straightness errors calculated by the analysis model are compared with the measured data, as shown in Fig. A.4, it is the good agreement between them that does verify the effectivity of the quasi-static analysis model.

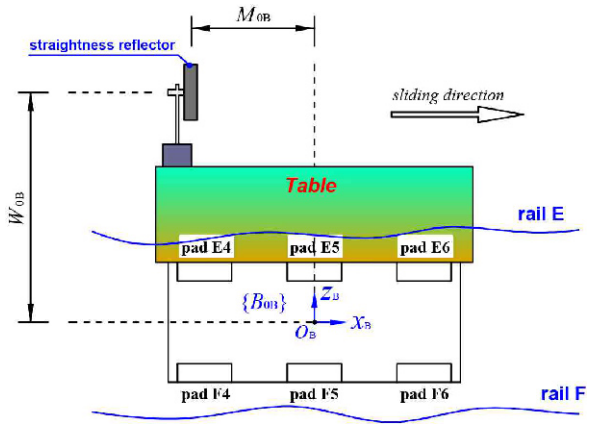

Fig. A.3. Location of the straightness reflector.

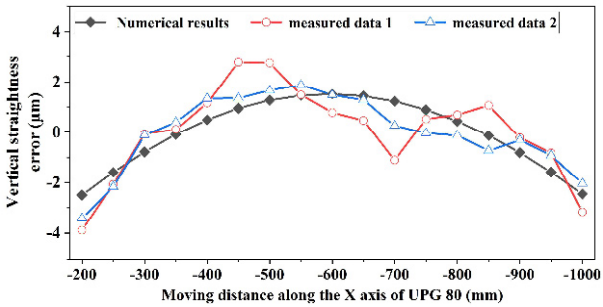

Fig. A.4. Comparison of the calculated vertical straightness errors and the measured data.

Chenchun Shi received his master degree from Ningbo University, Zhejiang, China. He is currently a postgraduate student pursuing the Ph.D. in Xiamen University (XMU), China. His research interest is mainly focused on precision engineering and manufacturing.

Zhenzhong Wang received his B.S and Ph.D. in mechanical engineering from Department of Mechanical and Electrical Engineering, Xiamen University in 2003 and 2009. He is currently an Associate Professor of mechanical engineering at Xiamen University. His current research interests include advanced optical manufacturing.

Yunfeng Peng received his Ph.D. in mechanical engineering from Harbin Institute of Technology in 2006. He is currently a Professor of mechanical engineering at Xiamen University. His current research interests include Intelligent Manufacturing, precision and ultraprecision machine tools, tribology, etc.